Acta Pharmaceutica Sinica B 2024;14(5):2097−2118

Chinese Pharmaceutical Association
Institute of Materia Medica, Chinese Academy of Medical Sciences

Acta Pharmaceutica Sinica B

www.elsevier.com/locate/apsb
www.sciencedirect.com

ORIGINAL ARTICLE

DDAH1 promotes neurogenesis and neural repair in cerebral ischemia

Qiming Gao[a,†], Pinfei Ni[a,†], Yilin Wang[b,†], Peiyun Huo[a], Xiaojie Zhang[c], Sihan Wang[a], Fuyao Xiao[a], Yixuan Li[a], Wei Feng[d], Juntao Yuan[d], Teng Zhang[e], Qiang Li[a], Boyu Fan[a], Yuhao Kan[a], Zhirui Li[a], Yimiao Qi[a], Junfei Xing[a], Zhenghong Yang[b], Haixiao Cheng[a], Xinran Gao[a], Xiaoyan Feng[f], Ming Xue[a], Yang Liu[c], Yumin Luo[b,*], Zhongbing Lu[d,*], Yuming Zhao[a,*]

[a]*Department of Pharmacology, School of Basic Medical Sciences, Capital Medical University, Beijing 100069, China*
[b]*Cerebrovascular Diseases Research Institute and Department of Neurology, Xuanwu Hospital of Capital Medical University, Beijing 100053, China*
[c]*State Key Laboratory for Structural Chemistry of Unstable and Stable Species, Institute of Chemistry, Chinese Academy of Sciences, Beijing 100190, China*
[d]*College of Life Science, University of Chinese Academy of Sciences, Beijing 100049, China*
[e]*Department of Laboratory Animal, School of Basic Medical Sciences, Capital Medical University, Beijing 100069, China*
[f]*Department of Physiology and Pathophysiology, School of Basic Medical Sciences, Capital Medical University, Beijing 100069, China*

Received 19 September 2023; received in revised form 21 December 2023; accepted 22 January 2024

KEY WORDS

DDAH1;
Neurogenesis;
Neural repair;
ChAT;
HIF-1α;
ACh;

Abstract Choline acetyltransferase (ChAT)-positive neurons in neural stem cell (NSC) niches can evoke adult neurogenesis (AN) and restore impaired brain function after injury, such as acute ischemic stroke (AIS). However, the relevant mechanism by which $ChAT^+$ neurons develop in NSC niches is poorly understood. Our RNA-seq analysis revealed that dimethylarginine dimethylaminohydrolase 1 (DDAH1), a hydrolase for asymmetric N^G,N^G-dimethylarginine (ADMA), regulated genes responsible for the synthesis and transportation of acetylcholine (ACh) (*Chat*, *Slc5a7* and *Slc18a3*) after stroke insult. The dual-luciferase reporter assay further suggested that DDAH1 controlled the activity of ChAT,

*Corresponding authors.
E-mail addresses: yumingzhao@ccmu.edu.cn (Yuming Zhao), luzhongbing@ucas.ac.cn (Zhongbing Lu), yumin111@ccmu.edu.cn (Yumin Luo).
†These authors contribute equally to the work.

Peer review under the responsibility of Chinese Pharmaceutical Association and Institute of Materia Medica, Chinese Academy of Medical Sciences.

https://doi.org/10.1016/j.apsb.2024.02.001

Stroke;
ADMA

possibly through hypoxia-inducible factor 1α (HIF-1α). KC7F2, an inhibitor of HIF-1α, abolished DDAH1-induced ChAT expression and suppressed neurogenesis. As expected, DDAH1 was clinically elevated in the blood of AIS patients and was positively correlated with AIS severity. By comparing the results among *Ddah1* general knockout (KO) mice, transgenic (TG) mice and wild-type (WT) mice, we discovered that DDAH1 upregulated the proliferation and neural differentiation of NSCs in the subgranular zone (SGZ) under ischemic insult. As a result, DDAH1 may promote cognitive and motor function recovery against stroke impairment, while these neuroprotective effects are dramatically suppressed by NSC conditional knockout of *Ddah1* in mice.

1. Introduction

Ischemic stroke is a leading cause of death worldwide, with an annual mortality rate of approximately 5.5 million people[1,2]. Moreover, almost half of survivors suffer from persistent poor functional outcomes with cognitive dysfunction[3-5]. Other than thrombolytics or tissue plasminogen activator (t-PA)[6], no effective drugs are available for acute stroke treatment. To date, many strategies for targeting the regeneration process and thereby decreasing disabilities after stroke have been explored.

DDAH1 has been previously investigated as a potential protective factor for cardiovascular diseases, nonalcoholic fatty liver disease and endothelium-related damage[7-11]. DDAH1 upregulates the level of nitric oxide (NO) by hydrolyzing ADMA, which is a competitive inhibitor of nitric oxide synthase (NOS)[12]. It has been proven that hyperhomocysteinemia and elevated hydrolyzing ADMA are risk factors for cardiovascular disease. Homocysteine can inhibit DDAH enzyme activity, causing the accumulation of ADMA and the inhibition of NO synthesis[10]. Our recent investigations indicated that cardiomyocyte DDAH1 is required for the metabolism of ADMA *in vivo*[7] and plays an important role in attenuating ventricular hypertrophy and dysfunction[13].

In addition to endothelial cells, neurons in the central nervous system could express DDAH1[14,15]. Recently, the functions of DDAH1 in neurological and psychiatric disorders, especially in stroke pathogenesis, were explored. Zhao et al.[16] demonstrated that DDAH1 improves cerebral ischemic tolerance after experimental cerebral ischemic insult *via* HIF-1 target genes. DDAH1 protects against blood−brain barrier leakage in the early phase of experimental cerebral ischemic stroke by regulating ADMA levels[14]. DDAH1 can attenuate cerebral ischemia impairment *via* the ROS/FOXO1/APR1 pathway[17]. In addition, an *in vitro* study by Wang et al.[18] revealed that DDAH1 participates in nerve growth factor (NGF)-induced neural differentiation in rat PC12 cells in an ADMA-independent manner, suggesting that DDAH1 might be involved in neurogenic actions through ADMA-independent pathways. A clinical survey by Ding et al.[15] reported that promoter polymorphism of *Ddah1* with a novel 4-nucleotide deletion/insertion variant is correlated with susceptibility to thrombotic stroke and coronary heart disease, which might be due to the functional loss of the ability to hydrolyze ADMA. Despite preliminary explorations of neuroprotection against AIS, the variations in DDAH1 expression in AIS patients and the inner rehabilitation response induced by DDAH1 are still obscure.

Adult neurogenesis (AN), an intrinsic process of generating newly formed integrated neurons from NSCs in the subventricular zone (SVZ) and SGZ, has been proven to restore impaired brain functions[19-21]. Hippocampal NSCs in the SGZ primarily generate dentate granule neurons that make up the bulk of the dentate gyrus (DG). The DG receives input from the entorhinal cortex, sending information through the trisynaptic circuit to CA3 and CA1, thus playing a critical role in learning and memory. Blocking new neuron formation disrupts cognitive performance, indicating that AN is a critical component of the hippocampal circuitry[22]. Several studies further support this notion and show that adult hippocampal neurogenesis generates neurons that are important for learning and memory, as well as for emotional regulation[23,24].

The process of neurogenesis, including the proliferation, survival and differentiation of NSCs into neurons, astrocytes and oligodendrocytes, is modulated by intrinsic and extrinsic factors[20,25-27]. Notably, the neurotransmitter ACh from $ChAT^+$ neurons can interact as an extracellular and niche-driven cue that controls neurogenesis in the SVZ and SGZ[26-31]. Mohapel et al.[28] reported that ACh in the forebrain promotes neurogenesis during the proliferation of NSCs in the SGZ. Veena et al.[29] showed that an agonist of the cholinergic muscarinic receptor can restore hippocampal neurogenesis, ameliorating cholinergic function loss. Further research by Paez-Gonzalez et al.[26] revealed a subset of $ChAT^+$ neurons in the SVZ niche that control the proliferation of NSCs, while blockade of nicotinic ACh receptors was found to exhibit the opposite effect[30,32]. However, the underlying mechanism through which $ChAT^+$ neurons can be formed and how ACh regulates the behaviors of NSCs should be further determined.

In the present study, DDAH1 levels in the blood of AIS patients were measured and found to be dramatically enhanced with the increase of AIS severity. To explore the effects and underlying mechanism of DDAH1 against AIS insult, the neurogenic activity of DDAH1 was explored in *Ddah1* TG mice and *Ddah1* KO mice *in vivo* and *in vitro*. We further constructed a Nestin-Cre cKO line in which *Ddah1* was knocked out in NSCs. After middle cerebral artery occlusion (MCAO) mimicked stroke insult in mice, DDAH1 expression was dramatically increased in brain regions and in blood, which was in line with the observations from clinical trials. As predicted, DDAH1 upregulated the proliferation and neural differentiation of NSCs after AIS insult. Enhanced neurogenic activity played a role in DDAH1-induced cognitive functional recovery, while knockout of *Ddah1* in NSCs or blockade of neurogenesis dramatically attenuated DDAH1-induced rehabilitation. Therefore, DDAH1 might regulate the proliferation of NSCs and their neural differentiation through the transcription factor HIF-1α, which controls the activity of *Chat* and the further synthesis of ACh.

2. Materials and methods

2.1. Materials

Antibody against DDAH1 for Western blotting was acquired from SAB (Shanghai, China). Antibodies against BrdU, doublecortin (DCX), neuronal nuclei (NeuN), 2′,3′-cyclic-nucleotide 3′-phosphodiesterase (CNPase), sex-determining region Y-box 2 (SOX2), postsynaptic density protein 95 (PSD95), Synapsin-1, S100β and glial fibrillary acidic protein (GFAP) for BrdU/GFAP/S100β costaining were purchased from Cell Signaling Technology (Danvers, MA, USA). Antibodies against nestin and GFAP for BrdU/GFAP costaining were purchased from Millipore (Billerica, MA, USA). Antibodies against glyceraldehyde-3-phosphate dehydrogenase (GAPDH) were obtained from Biosynthesis Biotechnology (Beijing, China). 4′,6-Diamidino-2-phenylindole (DAPI) was purchased from Beyotime Biotechnology (Shanghai, China). Antibodies against DDAH1 for immunofluorescence staining and antibodies against ChAT, CHRNA3 and CHRNB4 were obtained from Thermo Fisher Scientific (Waltham, MA, USA). Antibodies against BrdU for BrdU/GFAP/S100β costaining, arginine vasopressin receptor 1A (AVPR1A) and HIF-1α were obtained from Novus Biologicals (Centennial, CO, USA). Antibodies against synaptophysin, 3-nitrotyrosine (3-NT) and class III beta-tubulin (TuJ1) were purchased from Abcam (London, UK). Antibodies against GAP-43 were purchased from Santa Cruz Biotechnology (Dallas, Texas, USA).

Enzyme-linked immunosorbent assay (ELISA) kits for DDAH1 were purchased from Sinobest Bio (Shanghai, China). The qPCR RT Master Mix with gDNA Remover Kit was purchased from Toyobo (Shanghai, China). The BCA protein quantitation kit, protein marker, TRIzol, mix of real-time quantitative PCR, media and supplements used for cell culture were obtained from Thermo Fisher Scientific (Waltham, MA, USA). Temozolomide (TMZ), the α-conotoxin AuIB and KC7F2 were purchased from MedChemExpress (Shanghai, China). ACh detection kit was acquired from Nanjing Jiancheng Bioengineering Institute (Nanjing, Jiangsu, China). The enhanced chemiluminescence plus kit was purchased from Amersham Bioscience (Aylesbury, UK), and the phosphatase inhibitors cocktail and polyvinylidene fluoride membranes were obtained from Millipore Corporation (Billerica, MA, USA). Other reagents were obtained from Sigma−Aldrich (St. Louis, MO, USA). Nylon monofilament sutures for stroke induction were obtained from Doccol (Sharon, MA, USA).

2.2. Clinical subjects and sample collection

The Medical Ethics Committee of the Xuanwu Hospital of Capital Medical University granted ethical approval for this study (license No. [2021] 079). The study was performed in accordance with the Declaration of Helsinki. In the present survey, 150 AIS patients and 36 controls were enrolled. Our exclusion criteria were as follows: (1) history of AIS and (2) severe organic diseases such as malignant tumors and hepatic or renal dysfunction. Baseline information, including sex, age, previous history, laboratory test results and prognosis, was collected. In addition to the above-mentioned information, every patient was assessed according to the National Institute of Health Stroke Scale (NIHSS). AIS severity was evaluated based on NIHSS scores: slight AIS (NIHSS$\leq$4), moderate AIS (NIHSS ranges from 5 to 15), moderate to severe AIS (NIHSS ranges from 6 to 20) and severe AIS (NIHSS$\geq$21). Four milliliters of blood were collected within 24 h after the onset of AIS and before any intervention. Blood samples were centrifuged, and serum supernatants were obtained and stored at −80 °C until biochemical analysis. The samples were thawed before analysis, after which the significance of DDAH1 in AIS was assessed. DDAH1 levels were assessed *via* ELISA. Categorical variables in the clinical study were analyzed *via* the chi-square test and were presented as counts and percentages. Spearman's correlation test was performed to assess the relationship between DDAH1 and AIS severity[33]. Receiver operating characteristic (ROC) curve was generated to assess the diagnostic value of DDAH1 in AIS[34].

2.3. Experimental animals and induction of the mouse MCAO model

2.3.1. Animals

C57BL/6J mice were purchased from Beijing Vital River Laboratory Animal Technology (Beijing, China). *Ddah1* KO mice and homologous control *Ddah1*$^{flox/flox}$ (Flox) mice were obtained from the Jackson Laboratory as previously described[7,35]. *Ddah1* TG mice were generated by Cyagen Biosciences, Inc. (Nanjing, China) using an expression vector that contained an EF1A promoter, 3xFLAG/h *Ddah1* [ORF003160] and RNA processing signals from SV40. *Ddah1* TG mice were bred with wild-type C57BL/6J mice to generate *Ddah1* heterozygotes. To construct the Nestin-Cre *Ddah1* cKO line, Nestin-Cre (C57BL/6, Cg-Tg (Nes-Cre)1Kln/J) mice were kindly provided by Professor Jianwei Jiao from the Institute of Zoology, Chinese Academy of Sciences, as described previously[36,37]. Briefly, *Ddah1* Flox mice were hybridized with Nestin-Cre mice to generate *Ddah1*$^{flox/+}$; Nesin-Cre mice. *Ddah1*$^{flox/+}$; Nesin-Cre mice were subsequently hybridized with *Ddah1* Flox mice to obtain *Ddah1* cKO (*Ddah1*$^{flox/flox}$; Nesin-Cre) mice (Fig. 7A). Genotypings of the above mice were performed by polymerase chain reaction (PCR) of DNA from ear biopsy samples, the primers used were as follows:

Ddah1-Flox: 5′-AGGATGATCTGGACGAAGAGCA-3′ (forward), 5′-TTCTGAATCCCAGCCGT CTGAA-3′ (reverse);

Ddah1-flox-wt: 5′-AATCTGCA CAGAAGGCCCTCAA-3′ (forward), 5′-TTCTGAATCCCAGCCGTCTGAA-3′ (reverse);

Ddah1-ko: 5′-TGC AGGTCGAGGGACCTAATAACT-3′ (forward), 5′-AACCACACTGCTCG ATGAAGTTCC-3′ (reverse);

Ddah1-wt: 5′-AATCTGCA CAGAAGGCCCTCAA-3′ (forward), 5′-ATTGTTACAAGCCCTTAACGC-3′ (reverse);

hddah1: 5′-ATGCGATGGAGTTTCCCCACAC-3′ (forward), 5′-TGTCAT CGTCATCCTTGTAATCGA-3′ (reverse);

Internal control: 5′-CTATCAGGGAT ACTCCTCTTTGCC-3′ (forward), 5′-GGTTATTCAACTTGCACCATGC-3′ (reverse);

Nestin-Cre: 5′-GTCACTGTCGCCGCTACTTC-3′ (forward), and 5′-GGTTATTCAACTTGCACCATGC-3′ (reverse).

The results of genotyping were shown in Supporting Information Fig. S1.

2.3.2. Induction of the mouse MCAO model

All processes conformed to the guidelines of the Laboratory Animal Ethics Committee of Capital Medical University of China (license No. 2018-183). The animals were housed (12-h light/dark cycle) with access to food and water *ad libitum*. MCAO was performed as we described previously[38-42]. Briefly, the mice were placed in a supine position on a heating pad to maintain a constant rectal temperature (37 ± 0.5 °C). The right common carotid

artery, external carotid artery and internal carotid artery were isolated. Afterward, the common carotid artery was ligated, and a nylon monofilament suture was inserted from the external carotid artery to the internal carotid artery to reach the origin of the MCA. Blood flow in the MCA territory was monitored using a RFLSI III laser speckle Doppler flow meter (RWD Life Science, Shenzhen, Guangdong, China), which was placed perpendicular to the surface of the right parietal skull[43]. The changes in regional cerebral blood flow (rCBF) were expressed as percentages of the baseline values. Only mice whose rCBF decreased to 20%−30% of the baseline value during the ischemic period were considered to have successful ischemia[39]. Reperfusion was performed after the indicated ischemic interval, and the nylon filament was removed. The sham group was treated in the same way except for the occlusion of the MCA. Throughout the procedure, the room temperature was maintained at 24−25 °C.

2.4. BrdU incorporation and TMZ administration

BrdU incorporation assay is considered as the 'gold standard' for evaluating the neurogenesis activity. BrdU is a derivative of thymine and can be substituted for thymine to selectively integrate into newly synthesized DNA in cells, thus allowing DNA to be labeled during S phase[44]. In the present study, 50 mg/kg BrdU was administered on Days 0, 1 and 2 after ischemia by intraperitoneal (i.p.) injection[45]. TMZ is a DNA alkylating agent used to treat malignant glioma, and preclinical studies have shown a marked reduction in NSCs within the neurogenic niche in TMZ-treated mice[46]. To suppress the proliferation of NSCs potentiated by stroke insult, TG mice and WT mice were injected i.p. with TMZ during the first 3 days of the week for 4 consecutive weeks after MCAO as previously described[45].

2.5. Behavioral tests

2.5.1. Measurement of neurological score

The neurological deficits of the mice were measured on 0, 1, 2, 7, 14, 21 and 28 days after MCAO insult. Neurological deficits were evaluated on a four-point grading scale according to the Longa scoring system: a score of 0 indicated no neurological deficit; a score of 1 with forelimb flexion manifested a mild focal neurological deficit; a score of 2 with body circling to the left displayed a moderate focal neurological deficit; a score of 3 with body falling to the left showed a severe focal deficit; and a score of 4 indicated the inability to act spontaneously with a reduced level of consciousness[38].

2.5.2. Morris water maze test

On Day 24 after MCAO, the mice were trained in the Morris water maze device Pclab-300 (Panlab, Harvard Apparatus, USA). Briefly, mice were placed in a pool of water (1.2 m diameter, 19−20 °C) with 4 subdivided equal quadrants by imaging lines and a submerged escape platform (10 cm diameter, 2 cm below the water surface) located in the southeast quadrant. Briefly, animals were trained for 4 consecutive days with two trials per day (90 s per trial). Mice were allowed to swim for 90 s or until they found the platform, and the time to find the platform was recorded as the escape latency (a score of 90 s was assigned for mice that were unable to locate the platform). All the mice remained on the platform for 30 s after each trial. At the end of the learning paradigm, a probe trial (90 s) to measure the animals' memory of the platform position was tested. The percentage of time spent in each quadrant, duration in the goal quadrant, frequency in the southeast quadrant, frequency in the platform and velocity were recorded[45]. Swim paths were recorded using EthoVision XT 15 software (Noldus Information Technology, Beijing, China). Mice that could not swim after MCAO were excluded from the trial.

2.5.3. Rotarod assay

On Days 26−28 after MCAO, a rotarod test was performed as previously described[47]. On the first day, the mice were placed on a rotating rod (Panlab LE8205, Harvard Apparatus, USA) and spun at 4−5 rpm for adapted training. Each training session lasted for 3 min, and the interval between each trial was 15 min. On the second day, the rotation speed was adjusted to 14 rpm for 5 min, and all the mice were subjected to 3 trials on the first two days. On the third day, the periods that mice spent on the rotarod at a speed of 14 rpm before falling off were measured within 5 min for 3 times.

2.6. Histochemical staining

2.6.1. Tissue processing

As described previously[48], animals were anesthetized with 1% isoflurane and then perfused transcardially with 0.05 mol/L phosphate-buffered saline (PBS) (pH 7.4) followed by 4% paraformaldehyde solution. Brain tissues were removed and postfixed overnight at 4 °C. On the second day, the brain tissues were cryoprotected *via* 24 h of immersion in 20% sucrose. The brains were embedded in optimal cutting temperature (OCT) compound, and coronal cryosections were cut to a thickness of 20 μm.

2.6.2. Nissl staining

To assess brain damage, Nissl staining was performed as previously described[45]. Briefly, the frozen sections were washed with PBS three times and stained with cresyl fast violet dye for 20 min at room temperature. After being washed with distilled water and dehydrated in 95% ethanol and 100% ethanol, the slides were cleaned with xylene and mounted with neutral balsam.

2.6.3. Immunocytochemical staining

Brain sections were prepared in a '1 in 10' series as previously described[48]. After rinsing in PBS 3 times, the brain sections and cells were incubated in sodium citrate buffer at 90 °C for 20 min and then incubated with 1% Triton X-100 in 5% bovine serum albumin for 30 min. The sections were then exposed to the appropriate primary antibody for 72 h at 4 °C, followed by incubation at room temperature with the secondary antibody. The sections were incubated with DAPI for 10 min before images were captured. Immunofluorescence images were acquired by fluorescence microscopy.

2.7. 2,3,5-Triphenyltetrazolium chloride staining

Brains were sectioned into 1 mm coronal slices using a mouse brain matrix (RBM 4000C; ASI Instruments; Warren, MI, USA) and stained with 2% (*w/v*) 2,3,5-triphenyltetrazolium chloride (TTC) at 37 °C for 10 min[40]. The slices were scanned, and infarct areas were identified using an image analyzer (ImageJ System; National Institutes of Health; Bethesda, MD, USA). The infarct volume percentage was calculated from the following Eq. (1):

Infarct volume (%)=(Contralateral volume−Ipsilateral non-ischemic volume) × 100/Contralateral volume. (1)

2.8. Tissue collection

By observing the rCBF and TTC staining, we classified the ischemic regions as the penumbra and ischemic core, which mainly included the cortex and striatum. The distances of the infarct rims from the midline were measured[40]. TTC staining revealed that the lateral cortex region 1−2 mm from the midline of the coronal section, which fell within the border of the infarct area in the WT group, was the region that could be rescued. This area can thus be considered the ischemic penumbra. The ischemic cortex region that could not be rescued was considered the core region. Herein, the cortex from the ischemic core region and the striatum were collected. The DG containing the SGZ was included in the 'hippocampus' samples.

2.9. Western blot detection

Brain tissue samples were collected in RIPA cell lysis buffer supplemented with protease inhibitor cocktail and phosphatase inhibitors cocktail. Briefly, the striatum, hippocampus containing the SGZ and cortex from the ischemic core region were collected. The protein lysate was separated by sodium dodecyl sulfate−polyacrylamide gel electrophoresis and transferred onto a PVDF membrane. After blocking with 5% bovine serum albumin in TBST, the PVDF membranes were trimmed according to the molecular weight of the marker, and the primary antibodies were applied overnight at 4 °C. Secondary antibodies were then added, and the samples were incubated at room temperature for 2 h to facilitate the detection of protein expression *via* a chemiluminescence system. Blots were developed using an enhanced chemiluminescence plus kit, and images were acquired with a Bio-Rad XR Imaging Device (Hercules, CA, USA). Densitometric measurements of each membrane were performed using ImageJ software (National Institutes of Health, Bethesda, MD, USA)[45].

2.10. RNA-sequence assay and real-time quantitative PCR analysis

The hippocampus containing the SGZ from the ipsilateral hemisphere was collected from Flox and *Ddah1* KO mice at 24 h after ischemia. The tissues were then immediately frozen in dry ice and stored at −80 °C until RNA extraction. Total mRNA was isolated using TRIzol reagent. The amounts of RNA were determined by measuring optical density, and only RNA samples with an OD_{260}/OD_{280} ratio of 1.8−2.0 were used. Total RNA was reverse transcribed using qPCR RT Master Mix with a gDNA Remover Kit. cDNA construction and RNA sequencing were performed by Beijing Genomic Institution (BGI, Beijing, China). Differentially expressed genes (DEGs) with a threshold of 2-fold change ($|\log_2 FC| \geq 1$) and FDR<0.05 were chosen for analysis[49]. Gene Ontology (GO) and protein−protein interaction (PPI) analyses were subsequently performed. Signal networks were visualized with Cytoscape[50].

To validate the selected genes, total mRNA was extracted by using TRIzol reagent and cDNA was synthesized. Quantitative real-time PCR was performed using appropriate primers. Relative gene expression was calculated by the delta−delta Ct (^{DDCt}) method and converted to the relative expression ratio (2^{-DDCt}) for statistical analysis[51]. The data were normalized to the expression of the endogenous reference gene GAPDH. A dissociation curve (melting curve) was constructed in the range of 60−95 °C to evaluate the specificity of the amplification products. The results are presented as the fold change in mRNA levels[45]. The specific primers applied for identification were as follows:

Gng8: 5′-ATCGATCGCATGAAGGTGTC-3′ (forward), 5′-CTTGTCGCGGAAGGGATTC-3′ (reverse);

Chat: 5′-ACAGCCAATTGGGTCTCTGA-3′ (forward), 5′-GCCTTGTAGCT AAGCACACC-3′ (reverse);

Chrna3: 5′-TGC TTTACAACAACGCCGAT-3′ (forward), 5′-CCAGGTCGATCTTTGCCTTG-3′ (reverse);

Chrnb4: 5′-ACAGATCATGACCACCAGC A-3′ (forward), 5′-GTCCCATCGGCATTGTTG TA-3′ (reverse);

Avpr1a: 5′-CAGCAG CGTGAAGAGCATTT-3′ (forward), 5′-CGGA ATCGGTCCAAA CGAAA-3′ (reverse).

2.11. Determination of ACh concentration in brain tissue

After 1 day of ischemia, the ipsilateral hippocampus containing the SGZ was separated. Concentrations of ACh were determined by an assay kit from Nanjing Jiancheng Institute (Nanjing, Jiangsu, China) according to the manufacturer's instructions.

2.12. NSC isolation and cell culture

As described previously[49], NSCs were isolated from the hippocampi of E14-15 *Ddah1* KO, TG and WT mice. Briefly, mouse embryos were dissected, and the hippocampus was isolated in cold PBS containing 100 U/mL penicillin/streptomycin. Single cells were obtained by mechanical filtration through 70 μm nylon mesh. After centrifugation, the cells were resuspended in DMEM/F12. The dissociated cells were seeded at a density of 1×10^5 cells/mL in DMEM/F12 medium supplemented with 2% B27, 20 ng/mL recombinant human basic fibroblast growth factor and 20 ng/mL epidermal growth factor. Primary NSCs were kept in a humidified atmosphere of 5% CO_2 at 37 °C. Neurospheres appeared within a few days and were grown for 3−5 days before collection for passage. After two passages, the cells were used for the experiments. In addition, the growth factors basic fibroblast growth factor and epidermal growth factor were not present in the culture medium in the differentiation detection assay. All the experiments were approved by the Animal Care Facility of Capital Medical University, China.

2.13. OGD/R insult, drug treatment and RNA interference manipulation

NSCs were subjected to oxygen-glucose deprivation/reperfusion (OGD/R) to simulate ischemic conditions *in vitro*[52]. Briefly, NSCs were rinsed twice with PBS, after which the culture medium was replaced with glucose-free DMEM. The cells were cultured in a hypoxic chamber containing a mixture of 5% CO_2 and 95% N_2 for 1 h at 37 °C and reincubated in regular culture medium at 37 °C under normoxia. An inhibitor of HIF-1α (KC7F2) and an inhibitor of $\alpha 3\beta 4$ nAChR (α-conotoxin AuIB) were applied to NPCs after OGD/R insult. Short interfering RNA (silencing RNA, siRNA) and control RNA (scramble RNA) for *Chat* were synthesized by Sanon Biotech (Shanghai, China) as previously described[53]. After OGD/R insult, NPCs were transfected with *Chat* siRNA at a concentration of 100 nmol/L in serum-free DMEM/F12 with Lipofectamine 2000 reagent for 6 h. *Chat* scramble RNA was used as the control treatment. Cell proliferation was observed after

incubation for 24 h, and cell differentiation was observed after 5 days of culture.

2.14. *Luciferase reporter assay*

Chat activity was detected by a dual-luciferase reporter system (Beyotime, Shanghai, China)[54]. Cultured NSCs from *Ddah1* WT, KO and TG mice were transfected with Lipofectamine 2000 reagent with the reporter construct pGL4.27 containing the *Chat* gene promoter. The pRL-CMV plasmid, which expressed *Renilla* luciferase, was used as an internal control to normalize the transfection efficiency. All transfections were normalized to the total equal amount of DNA with the empty plasmid pGL4.27. To observe the regulation of *Chat* by HIF-1α, KC7F2 (20 μmol/L), an inhibitor of HIF-1α, was applied to NSCs isolated from *Ddah1* TG mice during and after transfection. Twenty-four hours after transfection, the cells were harvested, and the luciferase activity of *Chat* was measured using a SpectrMax M2e luminometer (Molecular Devices, San Jose, CA, USA).

2.15. *ELISA*

Blood samples of mice and blood from clinical subjects were collected and centrifuged at 3000 rpm (Sigma3k15, Sigma−Aldrich, St. Louis, MO, USA) for 15 min at 4 °C. The DDAH1 levels were measured using ELISA kits.

2.16. *Statistical analysis*

In the clinical study, compared with unpaired Student's *t* test or the Mann−Whitney U test, continuous variables are expressed as the mean or mean ± standard deviation (SD) for normally distributed data and medians for abnormally distributed data. Compared with the χ^2 test, categorical variables are expressed as numbers and percentages. ROC curve was generated with GraphPad Prism 8.0 (GraphPad Software, San Diego, CA, USA). Correlations between DDAH1 and other clinical indicators were estimated using Spearman's rank correlation coefficient and visualized *via* a heatmap generated with GraphPad Prism 8.0. For the preclinical study, all the data were reported as the mean ± standard error of mean (SEM). Statistical analysis was performed by two-way ANOVA with *post hoc* Dunnett's test or Student's *t* test for brain blood flow detection and the Morris water maze assay with GraphPad Prism 8.0. Other analyses were performed by one-way ANOVA with *post hoc* Dunnett's test or Student's *t* test with GraphPad Prism 8.0. The level of significance was considered at $^{*}P < 0.05$ and $^{**}P < 0.01$.

3. Results

3.1. *DDAH1 is enhanced in the blood of AIS patients after AIS impairment*

Our study consisted of 150 patients with AIS and 36 healthy controls. As shown in Supporting Information Table S1, no significant differences in age or sex were observed between the control and AIS groups. DDAH1 levels in blood were significantly different between the two groups. All patients were then divided into 4 groups based on NIHSS: slight AIS (NIHSS ≤4), moderate AIS (NIHSS ranging from 5 to 15), moderate to severe AIS (NIHSS ranging from 16 to 20), and severe AIS (NIHSS ≥21). The demographic features of 150 patients are summarized in Supporting Information Table S2. In addition to the DDAH1 level, age, atrial fibrillation status, white blood cell (WBC) count, neutrophil count and lymphocyte count differed significantly among the four groups.

DDAH1 levels in blood differed significantly between the control and AIS groups. The *P* value between the healthy control and the slight AIS group was 0.011, while the *P* values between the healthy control and the other 3 groups (moderate AIS, moderate to severe AIS and severe AIS) were all less than 0.001 (Fig. 1A). Next, ROC curve and the area under the curve (AUC) were generated to evaluate the diagnostic value of DDAH1 in AIS (Fig. 1B). When the cutoff value was 3381.555 pg/mL, the corresponding sensitivity and specificity were 68.0% and 72.2%, respectively. Spearman's correlation test showed that DDAH1 levels correlated with AIS severity (Fig. 1C).

3.2. *Expressions of DDAH1 are increased in mouse cerebral regions and blood after the initiation of ischemia−reperfusion injury*

The clinical survey showed that the DDAH1 level in the blood of AIS patients varied depending on the severity of the AIS insult. This finding raised the question of whether DDAH1 is an endogenous protective response against stroke-induced stress. To address this issue, further investigations were performed in MCAO mice. DDAH1 expression in the blood was tested which was elevated until 28 days of reperfusion after ischemia (Supporting Information Fig. S2). DDAH1 expression in different brain regions, including the ischemic core region of the cortex and striatum as well as the ipsilateral hippocampus, was subsequently measured after MCAO insult (Fig. 2). As described, neurological grading by Longa scores showed that neurological deficits could be observed after 1 h of ischemia and 23 h of reperfusion (I1h/R23h) (Fig. 2B). After 1 h of ischemia, DDAH1 was upregulated in the ipsilateral ischemic cortex and striatum at 1 and 23 h of reperfusion, respectively (Fig. 2C−E), but its level was elevated only at 23 h in the ipsilateral hippocampus (Fig. 2F). Afterward, DDAH1 expression was further evaluated after different durations of ischemia. Interestingly, the expression of DDAH1 was further elevated in the ipsilateral hippocampus but not in the striatum when the duration of ischemia was extended from 1.5 to 2 h (Fig. 2G−K). That is, DDAH1 expression increased but might reach a plateau in the ipsilateral striatum with the extension of ischemia. However, the expression of DDAH1 in the ipsilateral hippocampus was correlated with the duration of ischemia. These findings might indicate that DDAH1 in the ipsilateral hippocampus responds sensitively to stroke-induced stress. DDAH1 might be controlled by negative feedback to prevent excess DDAH1 expression in the ipsilateral striatum. To elucidate the effects of DDAH1 against ischemic stroke, we established an MCAO model in *Ddah1* TG, *Ddah1* KO and WT mice in the following study. DDAH1 expression was increased in the hippocampus and blood in the WT group. Compared with that in the WT group, the expression of DDAH1 in the hippocampus and blood was significantly higher in the *Ddah1* TG mice, while it was almost completely abolished in the *Ddah1* KO mice after I1h/R23h insult (Fig. 2L−N). The following investigations were performed in the model to determine the neuroprotective mechanism of DDAH1 against ischemic insults.

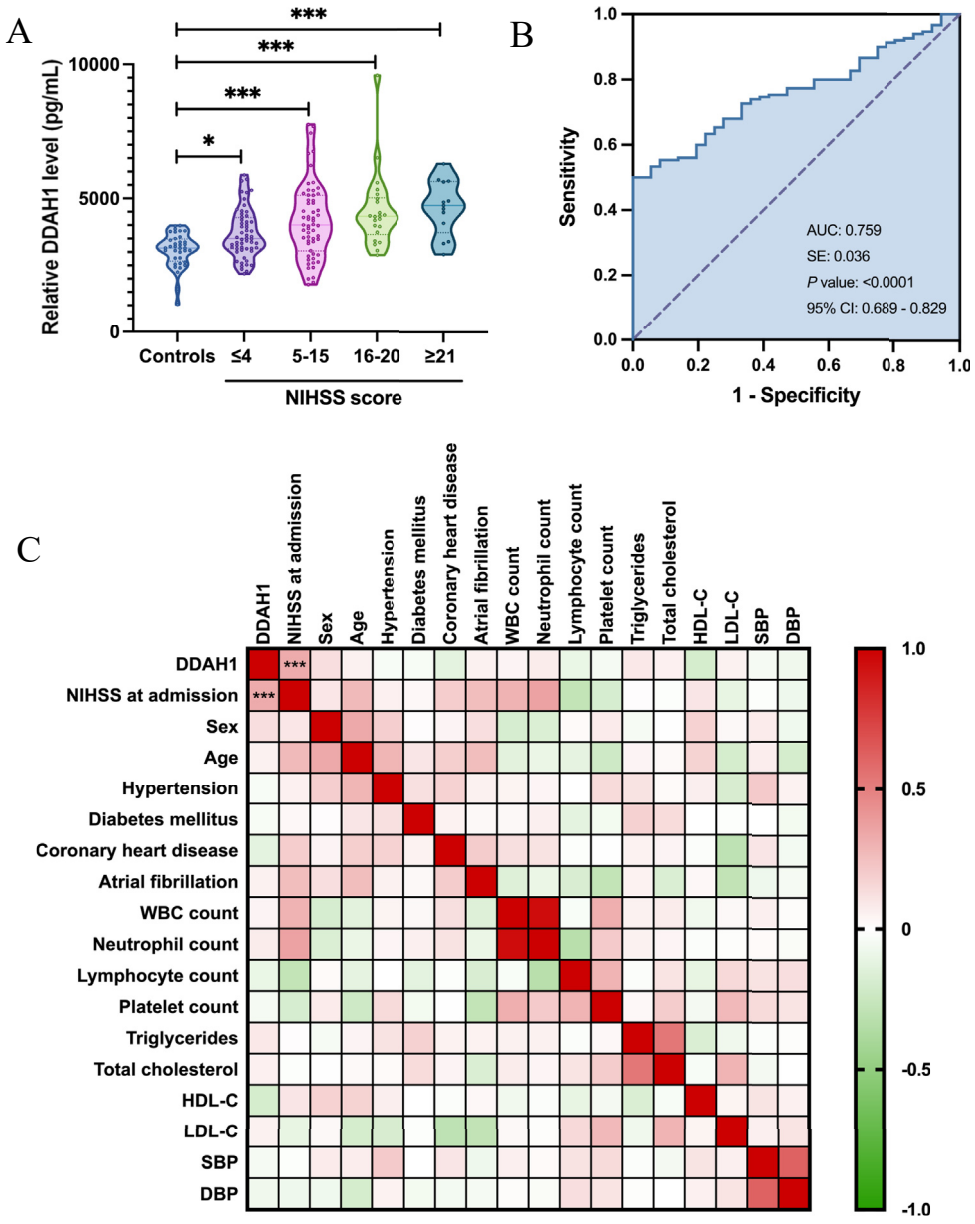

Figure 1 DDAH1 levels are elevated in the blood of AIS patients and are associated with the severity of AIS. (A) Violin plots depicting DDAH1 levels in the blood of the controls and patients, who were divided into 4 groups according to AIS severity. Controls ($n = 36$), patients with an NIHSS score≤4 ($n = 56$), 5≤NIHSS score≤15 ($n = 59$), 16≤NIHSS score≤20 ($n = 22$) and NIHSS score≥21 ($n = 13$). The lines correspond to the minima, maxima, centers and quartiles. *$P < 0.05$, ***$P < 0.001$ *versus* the control group; one-way ANOVA with Dunnett's multiple comparisons test. (B) ROC curve for the serum DDAH1 concentration to predict the diagnosis of AIS (AUC = 0.759, 95% confidence interval = 0.689−0.829, $P < 0.001$). (C) Spearman's correlation heatmap analysis of DDAH1 expression, NIHSS score at admission and other clinical indicators. Red represents a positive correlation, and green represents a negative correlation. DDAH1 levels were positively correlated with NIHSS scores at admission (***$P < 0.001$). HDL-C: high-density lipoprotein cholesterol; LDL-C: low-density lipoprotein cholesterol; SBP: systolic blood pressure; DBP: diastolic blood pressure.

3.3. DDAH1 promotes the proliferation and neuronal fate commitment of NSCs after the onset of ischemia−reperfusion injury

To determine whether DDAH1 could induce regeneration in response to stroke insult, the neurogenic activities of the *Ddah1* KO, *Ddah1* TG and WT strains were compared. The results showed that DDAH1 promoted the proliferation of NSCs after the onset of ischemia−reperfusion injury. First, immunostaining analysis confirmed that DDAH1 was expressed in Nestin^{+} cells in the SVZ and SGZ after MCAO insult, indicating that DDAH1 was expressed in NSCs (Fig. 3A and B). Second, BrdU incorporation assay was performed from Day 0 to Day 2 after ischemic stroke to determine the effects of DDAH1 on neurogenesis (Fig. 3C−E). Compared with those in sham-operated mice, the number of BrdU^{+}DCX^{+} cells, which represent proliferated NSCs, was significantly increased in the SVZ and SGZ of ipsilateral brains in the WT group after MCAO insult. This trend was reversed in KO

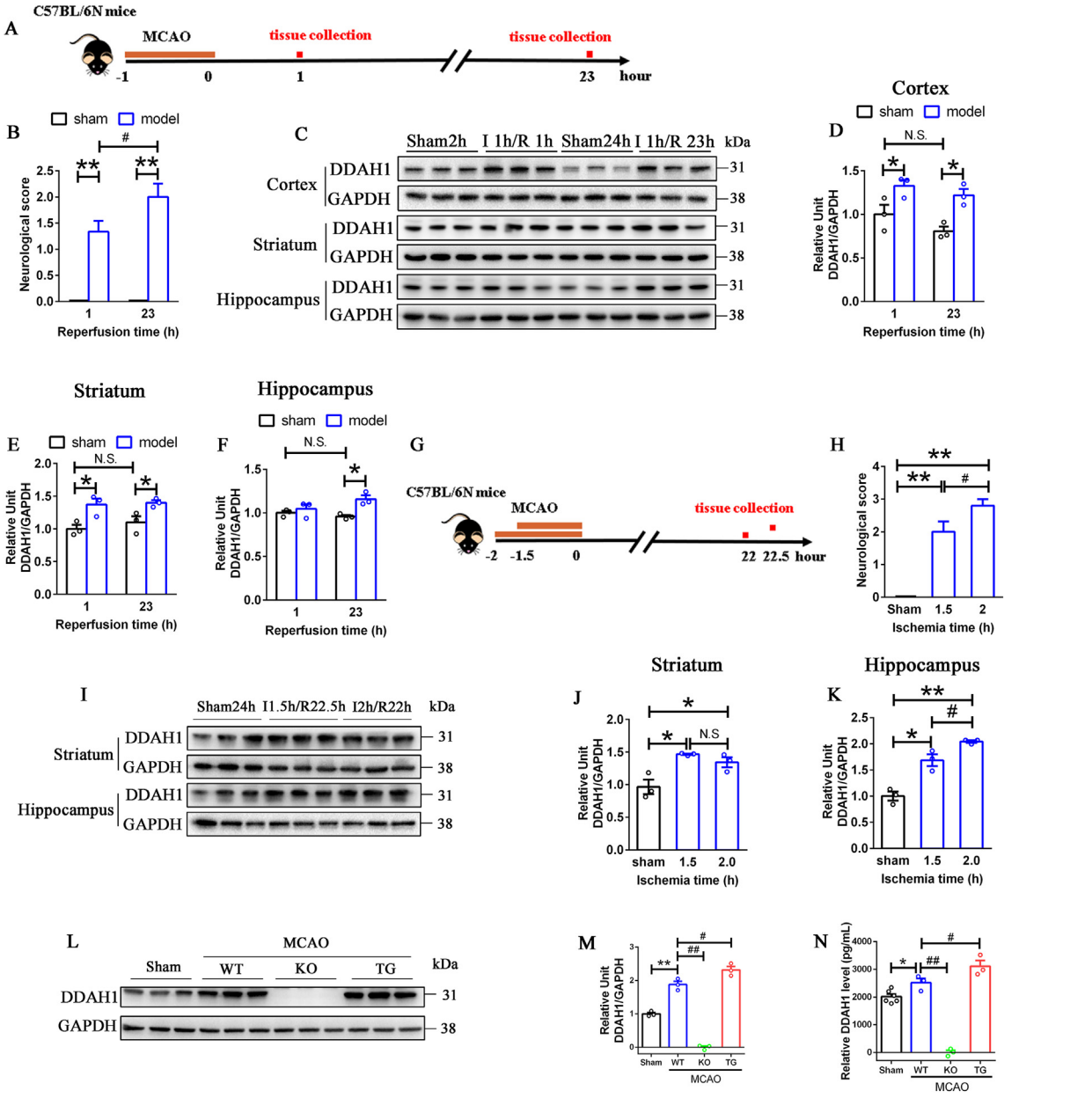

Figure 2 Expression levels of DDAH1 are increased in various brain regions within 24 h of ischemia/reperfusion injury. (A) Experimental illustration of the MCAO model in WT mice. Brain tissues were collected for Western blotting analysis after 1 h of ischemia followed by 1 h of reperfusion (I1h/R1h) and I1h/R23h. (B) Evaluation of neurological deficits by the Longa scoring system poststroke ($n = 6$ per group). The values are shown as the mean ± SEM. $^{**}P < 0.01$ *versus* the sham group; $^{\#}P < 0.01$ *versus* the I1h/R1h group; two-way ANOVA with Dunnett's multiple comparisons test. (C) Representative bands in Western blotting assays of DDAH1 expression in the ipsilateral ischemic cortex, striatum and hippocampus after I1h/R1h and I1h/R23h. (D−F) Quantitative analysis of DDAH1 expression in the ipsilateral ischemic cortex (D), striatum (E), and hippocampus (F) ($n = 3$ per group). The values are shown as the mean ± SEM. $^{*}P < 0.05$ *versus* the sham group, n.s. indicates no significance; two-way ANOVA with Dunnett's multiple comparisons test. (G) Experimental illustration of the MCAO model in which the ischemia interval was extended from 1.5 to 2 h in WT mice. Brain tissues were collected for Western blot analysis after 1.5 h of ischemia followed by 22.5 h of reperfusion (I1.5 h/R22.5 h) and after 2 h of ischemia followed by 22 h of reperfusion (I2h/R22h). (H) Evaluation of neurological deficits by the Longa scoring system poststroke ($n = 6$ per group). The values are shown as the mean ± SEM. $^{**}P < 0.01$ *versus* the sham group; $^{\#}P < 0.05$ *versus* the I1.5 h/R22.5 h group; one-way ANOVA with Dunnett's multiple comparisons test. (I) Representative bands of Western blotting assays of DDAH1 expression in the ipsilateral striatum and hippocampus after I1.5 h/R22.5 h and I2h/R22h. (J, K) Quantitative analysis of DDAH1 expression in the ipsilateral striatum (J) and hippocampus (K) ($n = 3$ per group). The values are shown as the mean ± SEM. $^{*}P < 0.05$, $^{**}P < 0.01$ *versus* the sham group; $^{\#}P < 0.05$ *versus* the I1.5 h/R22.5 h group, n.s. indicates no significance; one-way ANOVA with Dunnett's multiple comparisons test. (L) Western blotting results showing DDAH1 expression in the ipsilateral hippocampus after I1h/R23h injury. (M) Quantitative analysis of DDAH1 expression in the ipsilateral hippocampus. (N) Levels of DDAH1 in the blood of MCAO mice after I1h/R23h were detected ($n = 6$ in sham group, $n = 3$ in WT, KO and TG groups). The values are shown as the mean ± SEM. $^{*}P < 0.05$, $^{**}P < 0.01$ *versus* the sham group; $^{\#}P < 0.05$, $^{\#\#}P < 0.01$ *versus* the WT group; one-way ANOVA with Dunnett's multiple comparisons test.

mice, in which the number of proliferated NSCs almost declined to a level similar to that of sham-operated mice. Conversely, the TG mice exhibited the opposite trend: there were more colabeled cells in the SVZ and SGZ than in the WT mice.

Further study revealed that DDAH1 induced neuronal fate commitment in the hippocampus after ischemia−reperfusion injury. To determine whether DDAH1 could control the differentiation of NSCs poststroke, we performed double immunostaining for BrdU and NeuN (a marker of mature neurons). The results showed that a number of NSCs were driven to the neuronal lineage in the ipsilateral striatum and DG at 28 days after ischemia-reperfusion injury (Fig. 4). Although DDAH1 strongly promoted the regulation of neural differentiation of NSCs in the SVZ, there was no significant difference between the WT and KO groups (Fig. 4A−C). In contrast, knockout of *Ddah1* decreased the number of mature neurons, and overexpression of DDAH1 in TG mice increased the number of mature neurons in the DG after ischemic insult (Fig. 4B−D).

In addition to BrdU^{+}NeuN^{+} cells, there were certain BrdU^{+} cells whose fates were unclear after ischemic insult. To explore

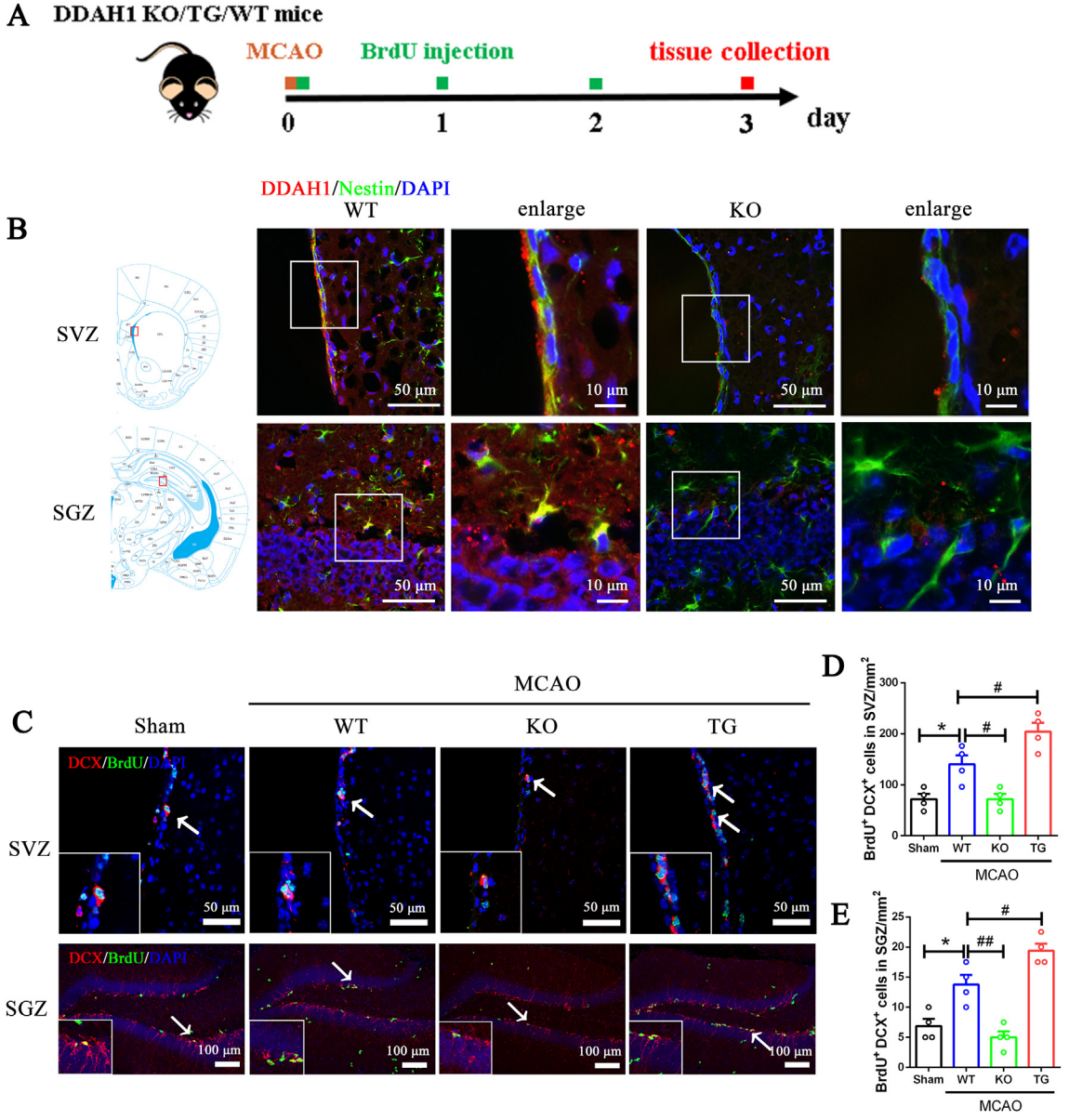

Figure 3 DDAH1 promotes the proliferation of NSCs under ischemic insult. (A) Experimental design for the proliferation of NSCs after 1 h of ischemia followed by 3 days of reperfusion (I1h/R3d). BrdU was added twice a day for the first 2 days after ischemia (50 mg/kg). (B) Representative images of double-label immunofluorescence staining for DDAH1 and Nestin in the ipsilateral SVZ and SGZ. The brain locations used were established according to the Mouse Brain Stereotaxic Coordinates of Paxinos and Franklin (4th Edition, Academic Press, Inc., 2013; New York, USA). Coordinate of the SVZ: +1.21 mm from the Bregma point Coordinate of the SGZ: −2.53 mm from the Bregma Point. (C) Representative images of double-label immunofluorescence staining for BrdU and DCX in the ipsilateral SVZ and SGZ. (D, E) Statistical analysis of BrdU^{+}DCX^{+} cells in the ipsilateral SVZ (D) and SGZ (E) ($n = 4$ per group). The values are shown as the mean ± SEM. *$P < 0.05$ *versus* the sham group; $^{\#}P < 0.05$, $^{\#\#}P < 0.01$ *versus* the WT group; one-way ANOVA with Dunnett's multiple comparisons test.

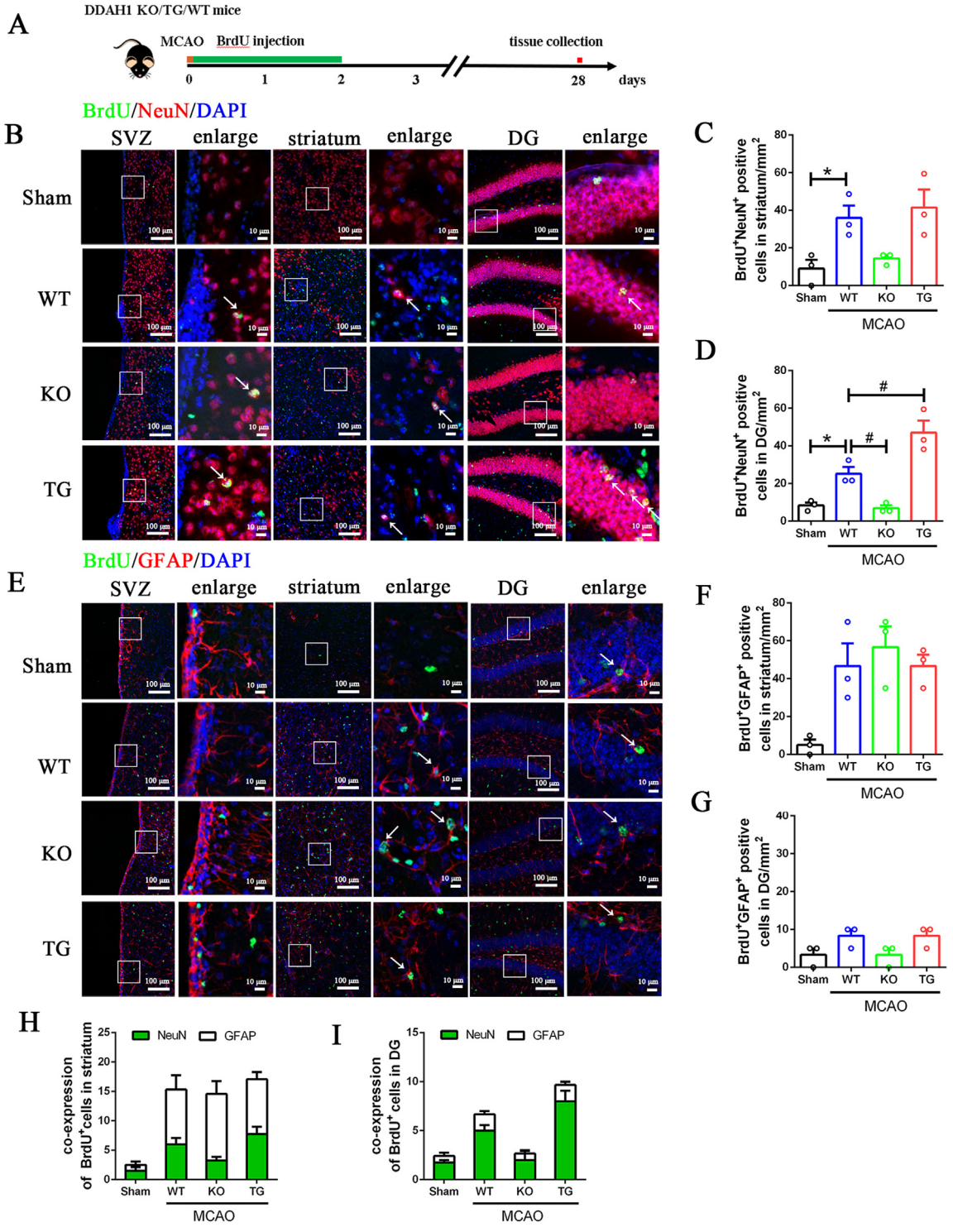

Figure 4 DDAH1 promotes the neural differentiation of NSCs under ischemic insult. (A) Experimental design for the differentiation of NSCs after I1h/R28d. BrdU was treated twice a day for the first 2 days after ischemia (50 mg/kg). (B) Representative images of double-label immunofluorescence staining for BrdU and NeuN in the ipsilateral SVZ, striatum and DG. (C, D) Statistical analysis of $BrdU^+NeuN^+$ cells in the ipsilateral striatum (C) and DG (D). (E) Representative images of double-label immunofluorescence staining for BrdU and GFAP in the ipsilateral SVZ, striatum and DG. (F, G) Statistical analysis of $BrdU^+GFAP^+$ cells in the ipsilateral striatum (F) and DG (G). (H, I) Summarization of the cells colabeled with BrdU and biomarkers for neurons (NeuN) and astrocytes (GFAP) in the striatum (H) and DG (I), respectively. The values are shown as the mean ± SEM in (C), (D), (F), (G), (H), and (I) ($n = 3$ per group). $^*P < 0.05$ *versus* the sham group; $^{\#}P < 0.05$ *versus* the WT group; one-way ANOVA with Dunnett's multiple comparisons test.

this issue, we further performed a study in which GFAP (a biomarker of astrocytes) and CNPase (a biomarker of oligodendrocytes) were colabeled with BrdU in the SVZ and SGZ, respectively. After 28 days of stroke insult, BrdU$^+$GFAP$^+$ cells were observed in the striatum and DG adjacent to the SVZ, but no significant difference was observed among the KO, TG, and WT groups (Fig. 4E−G). In addition, BrdU$^+$CNPase$^+$ cells were seldom observed in the ipsilateral striatum or DG (Supporting Information Fig. S3). After summarizing the above results of the BrdU-coexpressed cells, we found that DDAH1 did not affect the total number of BrdU$^+$ cells in the SVZ or the adjacent striatum (Fig. 4H). However, DDAH1 did affect the total number of BrdU$^+$ cells in the DG (Fig. 4I). The majority of BrdU$^+$ cells might have differentiated into astrocytes, and only a small portion may have differentiated into neurons in the SVZ, which later migrated into the adjacent striatum. Nonetheless, DDAH1 might determine the neural fate of NSCs in the DG region since the majority of BrdU$^+$ cells colocalized with NeuN after stroke insult (Fig. 4I).

In summary, DDAH1 in NSCs regulated neurogenic behaviors after ischemic insult. It promoted the proliferation of NSCs in the SVZ and SGZ but determined only the neuronal fate commitment of NSCs in the SGZ after stroke impairment.

3.4. DDAH1 participates in cognitive and motor rehabilitation partially by activating endogenous neurogenesis after stroke impairment

To explore whether the elevated neurogenesis induced by DDAH1 could ultimately contribute to the recovery from stroke insult, neurological deficit grading was performed *via* the Longa scoring system, Morris water maze test and rotarod test (Fig. 5A−I). Knockout of DDAH1 aggravated neurological deficits and decreased cognitive and motor function after 28 days of stroke insult. Morphological observation *via* Nissl staining revealed that stroke insult caused pyknotic cells and cytoplasmic chaos in the cortex and striatum (Supporting Information Fig. S4). Compared with those in WT mice, KO manipulation might have induced more severe impairments, while TG manipulation might have decreased the number of nuclear pyknotic cells and the degree of cytoplasmic chaos in the indicated regions. In addition, cell densities in the SGZ of the DG were more intensive in the TG group than in the WT group, while the opposite trend was observed in the KO group. Taken together, these results showed that upregulation of DDAH1 might promote the proliferation and neural differentiation of NSCs and contribute to neurological function improvement poststroke.

TMZ, a proliferation inhibitor of neurogenesis, was i.p. injected into TG and WT mice to further determine the effects of neurogenesis on DDAH1-induced neuroprotection after ischemic stroke. Stroke could upregulate endogenous neurogenesis. However, this increase in neurogenesis is not sufficient to repair the impaired brain. In our study, endogenous neurogenesis was mild so that TMZ did not induce dramatic adverse effects on the learning function of MCAO mice when it was used to block neurogenesis. TMZ might have a mild effect on memory function since it decreased the number of arrivings at the platform in the probe trial assay (Fig. 6G). In TG mice, TMZ strongly abolished DDAH1-promoted neuroprotection and cognitive function recovery at 28 days after stroke onset (Fig. 6A−H). However, TMZ did not abolish DDAH1-induced motor function recovery (Fig. 6I). Immunostaining assays showed that TMZ significantly decreased the number of BrdU$^+$NeuN$^+$ cells in the striatum and DG of TG mice (Fig. 6J−L). Cognitive functions are strongly related to the biological activities of the hippocampal region, while motor functions are related to the actions of the striatum. The results of histochemical staining showed that DDAH1 might promote the proliferation of NSCs in the SVZ and SGZ but may enhance neural differentiation only in the SGZ, which in turn indicated that DDAH1 might produce a more intensive effect in the SGZ than in the SVZ. Thereafter, we focused on the effects of DDAH1 on neurogenesis in the SGZ.

To verify whether newborn neurons derived from NSCs can form mature neurons and be integrated into impaired tissue, the expression of synapse-associated proteins in the ipsilateral hippocampus was measured. DDAH1 KO decreased the expression of the presynaptic proteins synapsin-1 and synaptophysin, the postsynaptic protein PSD95 and the axon biomarker GAP43. In contrast, the opposite trend was observed for these proteins in *Ddah1* TG mice (Fig. 5J−N). TMZ significantly decreased the enhanced expression of synapsin-1, synaptophysin and GAP43, which was induced by *Ddah1* TG manipulation. However, TMZ only partially abolished the enhanced expression of PSD95 in TG mice (Fig. 6M−Q), indicating that neurogenesis only contributed to postsynapse formation. TMZ decreased the synapse-related proteins synaptophysin, PSD95 and GAP43 in WT mice in the MCAO group (Fig. 6R−V). These investigations suggested that DDAH1 promotes neurogenesis in the hippocampus, which partially rescues synaptic deficits and neurological deficits after stroke insult.

3.5. Conditional knockout of Ddah1 in NSCs inhibits stroke-induced neurogenesis and worsens functional impairment

In the above investigations, we proved that DDAH1 could regulate the proliferation and neural differentiation of NSCs, which contributed to the functional recovery of ischemic stroke. However, the types of cells in which DDAH1 plays a major role in the NSC niche have not been identified. To investigate this issue, cKO of *Ddah1* in NSCs was established to determine the effects of DDAH1 on neurogenesis after ischemic stroke (Fig. 7A). Compared with those in the Flox group, the cell fate of BrdU$^+$ cells in the SVZ and adjacent striatum was not altered in the cKO group. Conversely, cKO significantly altered the number and neural fate determination of BrdU$^+$ cells in the SGZ of the DG (Fig. 7B−F). Compared with that in the Flox group, the number of BrdU$^+$NeuN$^+$ cells in the cKO group was dramatically lower. But there was no difference in the number of BrdU$^+$GFAP$^+$ cells between the cKO group and the Flox group in both the SVZ region and the SGZ region. As expected, cKO *Ddah1* aggravated neurological deficits and impaired the cognitive and motor function 28 days after stroke insult (Fig. 7G−N). cKO *Ddah1* exhibited decreased expression of the presynaptic proteins synapsin-1 and synaptophysin, the postsynaptic protein PSD95 and the axon biomarker GAP43 (Fig. 7O−S). Taken together, these findings indicated that DDAH1 in NSCs in the SGZ region regulates neurogenic activity in the hippocampus and further functional recovery.

3.6. DDAH1 activates multiple regeneration-guiding factors, including chat, after early ischemic insult

Previous studies have proven that the DDAH1/ADMA/HIF-1 pathway contributes to neuroprotection against acute ischemic insults[14,16]. However, whether DDAH1 can exert regenerative effects against stroke insults and the underlying mechanism

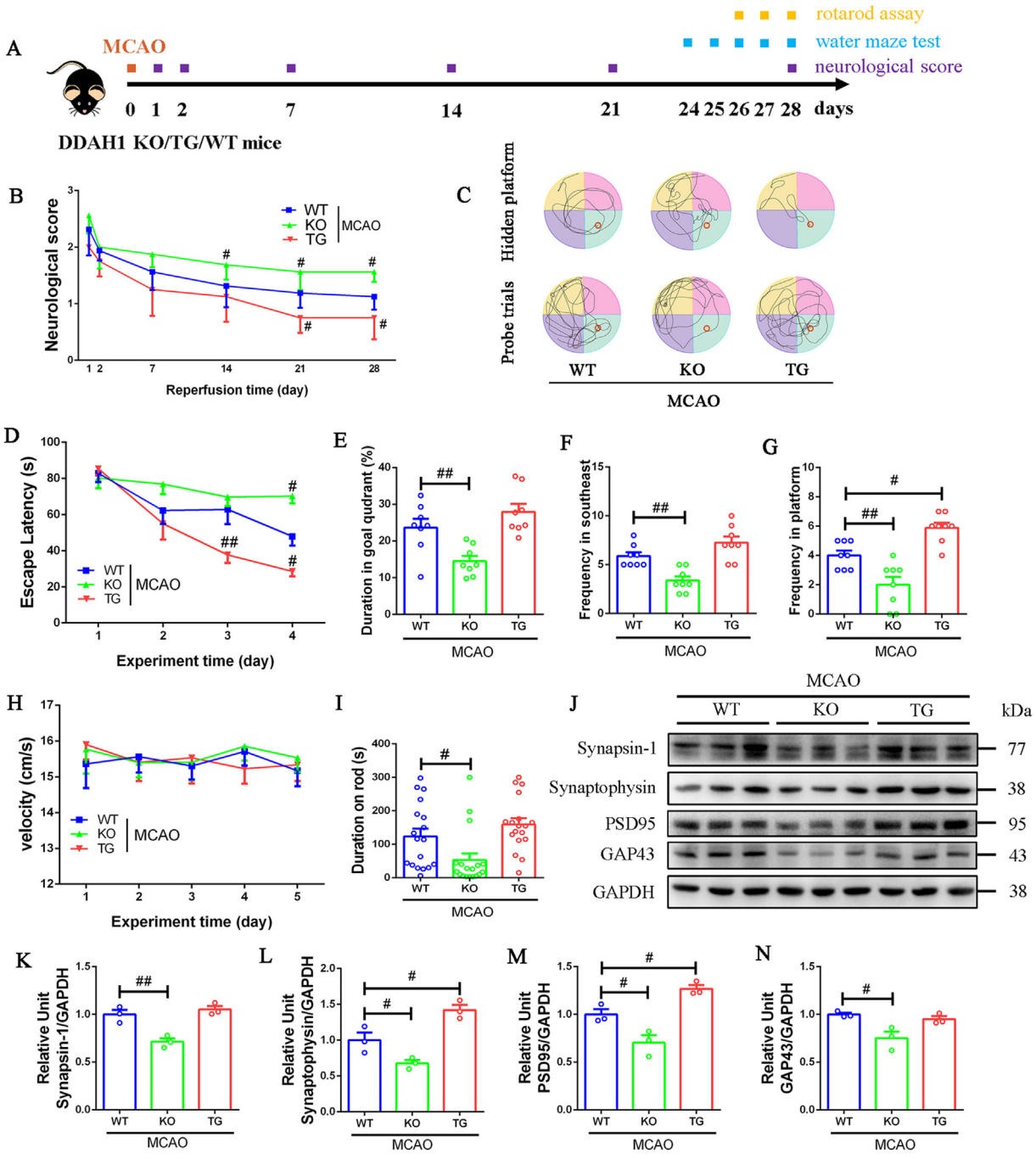

Figure 5 DDAH1 promotes cognitive rehabilitation after I1h/R28d and regulates the expression of synapse-associated proteins. (A) Experimental design for assessing cognitive and motor functions in *Ddah1* KO, TG and WT mice after I1h/R28d impairment. Cognitive functions were evaluated *via* the Morris water maze test from Day 24 to Day 28 postischemia, while motor functions were evaluated *via* the rotarod test from Day 26 to Day 28 postischemia. (B) Evaluation of neurological deficits by the Longa scoring system poststroke at the indicated times ($n = 8$ per group). The values are shown as the mean ± SEM. $^{\#}P < 0.05$ *versus* the WT group; two-way ANOVA with Dunnett's multiple comparisons test. (C) Representative swimming tracks to the hidden platform on Day 27 and the probe trial test on Day 28 poststroke. (D) Cognitive functions were assessed by the escape latency in the Morris water maze test from Day 24 to Day 27 after ischemia ($n = 8$ per group). The values are shown as the mean ± SEM. $^{\#}P < 0.05$, $^{\#\#}P < 0.01$ *versus* the WT group; two-way ANOVA with Dunnett's multiple comparisons test. (E–G) Spatial bias (E), frequency in the southeastern quadrant (*i.e.*, platform-located quadrant) (F) and frequency in the platform (G) were detected on Day 28 in the probe trial survey after ischemia. (H) Swimming speed of the mice within 5 days of the Morris water maze test. The speed was not significantly different among the testing groups, indicating that the difference in learning and memory function among the groups was not due to motor dysfunction. (I) Motor coordination was evaluated by the rotarod test. The latency to fall from the instrument was measured 3 times per mouse on Day 28 postischemia ($n = 6$ per group). The values are shown as the mean ± SEM. $^{\#}P < 0.05$, $^{\#\#}P < 0.01$ *versus* the WT group; one-way ANOVA with Dunnett's multiple comparisons test. (J) Representative Western blot showing the expression of the synapse-associated proteins

remain elusive. Therefore, RNA-seq assay and bioinformatics analysis were performed in this study. A total of 195 DEGs were identified in the ipsilateral hippocampus between WT mice and *Ddah1* KO mice after I1h/23R insult (Fig. 8A). Among the DEGs, 85 were upregulated and 110 were downregulated in KO mice (Fig. 8B). Seven nerve function-related biological processes and six ACh-associated molecular functions were identified which were among the top 20 terms according to the GO analysis (Supporting Information Fig. S5). PPI bioinformatics analysis indicated that the key DEGs regulated by DDAH1 were mainly involved in inflammation and nerve generation (Fig. 8C). For instance, chemokine ligand 7 (*Ccl7*) is the most intensive DEG that can induce a variety of immune responses. The nerve generation-associated genes, which included ACh synthesis-related genes (*Chat*, *Slc18a3*, *Slc5a7*), $\alpha3\beta4$ nicotinic cholinergic receptor ($\alpha3\beta4$ nAChR) signal-related genes (*Chrna3*, *Chrnb4* and *Gng8*) and *Avpr1a* signal-related genes (*Avpr1a* and *Gng8*), were regulated by DDAH1 (Fig. 8D).

To determine the effects of DDAH1 on regeneration after ischemic stroke, the expression of the DEGs was further verified in WT, *Ddah1* KO, TG, Flox and Nestin-Cre cKO mice. Real-time qPCR and Western blot analyses revealed that DDAH1 dramatically downregulated the expression of ChAT and nAChR subunits $\alpha3$ and $\beta4$ in KO mice (Fig. 8E–J). The concentration of ACh in the hippocampus was lower in the KO group than in the WT group (Fig. 8K). cKO-mediated manipulation of DDAH1 dramatically downregulated the expression of ChAT and the nAChR subunits $\alpha3$ and $\beta4$ compared with that in the Flox group (Fig. 8L–P). However, manipulation of DDAH1 in cKO mice altered only the expression of *Avpr1a* at the mRNA level (Fig. 8L, M and Q). As expected, the concentration of ACh in the hippocampus was lower in cKO mice than in Flox mice (Fig. 8R). These results suggest that DDAH1 regulates cholinergic signals and is an active player in the regeneration process.

3.7. *ChAT contributes to DDAH1-promoted proliferation and neural fate decision in NSCs through the transcription factor HIF-1α*

To address the regulation of cholinergic signals by DDAH1, ChAT and SOX2 were investigated *in vivo*. The results revealed that the number of ChAT$^+$SOX2$^+$ cells was significantly increased in the SVZ and SGZ after ischemia (Fig. 9). The number of ChAT$^+$SOX2$^+$ cells was decreased in *Ddah1* KO mice, while TG manipulation of *Ddah1* induced the opposite effect. cKO manipulation of *Ddah1* in NSCs partially abolished the ischemia-induced increase in ChAT$^+$SOX2$^+$ cells in the SGZ region.

To analyze the role of DDAH1 in neurogenesis, DDAH1 expression in NSCs from isolated embryonic hippocampi was evaluated. In line with the results obtained from the *in vivo* study, DDAH1 was expressed in the isolated NSCs. Compared with those in the WT group, the expression of DDAH1 in NSCs was lower in the KO group, while TG manipulation had the opposite effect (Supporting Information Fig. S6A and S6B). BrdU and SOX2 colabeling showed that DDAH1 controlled the proliferation of NSCs following OGD insult. The results showed that KO decreased the fluorescence intensities of SOX2 and BrdU as well as the number of SOX2$^+$BrdU$^+$ cells, while TG manipulation reversed these effects (Fig. S6C–S6E).

Previous studies had indicated that DDAH1 might regulate the expression of HIF-1α during ischemic insult.[16] Bioinformatic analysis *via* JASPAR, a database predicting transcription factor/protein binding profiles, suggested that HIF-1α binds to the promoter of *Chat*. Herein, we propose that DDAH1 regulates neurogenesis through HIF-1α/*Chat* signaling. The dual-luciferase reporter assay confirmed that *Chat* activity was enhanced in NSCs isolated from *Ddah1* TG mice, while the opposite trend was observed in NSCs isolated from *Ddah1* KO mice. KC7F2, an inhibitor of HIF-1α, significantly inhibited DDAH1-upregulated ChAT activity in NSCs from *Ddah1* TG mice (Fig. S6F). As proposed, DDAH1 regulated the expression of HIF-1α and ChAT in NSCs, while the HIF-1α inhibitor KC7F2 decreased the expression of HIF-1α and ChAT as well as the number of ChAT$^+$HIF-1α^+ cells (Fig. S6G–S6I).

To further analyze the role of ChAT in DDAH1-regulated neurogenic activity, coimmunostaining of NSCs with ChAT and SOX2 was performed. DDAH1 controlled the expression of ChAT and SOX2 in NSCs after OGD/R injury (Supporting Information Fig. S7A–S7D). *Ddah1* KO reduced the number of ChAT$^+$SOX2$^+$ cells as well as the intensity of SOX2, while TG manipulation induced the opposite trends. KC7F2 and RNA interference with *Chat* abolished the expression of SOX2 and the number of ChAT$^+$SOX2$^+$ cells, respectively. These results indicated that HIF-1α/*Chat* signaling may participate in the DDAH1-promoted proliferation of NSCs**.**

Although DDAH1 promoted the neuronal differentiation of NSCs in the hippocampus (Fig. 4), whether this differentiation was dependent on the enhanced proliferation of NSCs was unknown. Therefore, the effects of DDAH1 on the determination of the neural fate of NSCs were determined *in vitro*. When cultured in differentiation medium lacking growth factors, NSCs gradually differentiated under OGD/R insult (Fig. S7E). DDAH1 controlled neural differentiation and neurite extension. Both the number of ChAT$^+$ cells and the expression of ChAT in differentiated neurons were in line with the variation in DDAH1 expression observed in OGD/R injury (Fig. S7F–S7H). KC7F2 and RNA interference inhibited the number of ChAT$^+$TuJ1$^+$ cells as well as the intensities of ChAT and TuJ1. Taken together, these data indicated that HIF-1α/*Chat* signaling might play a role in the DDAH1-mediated promotion of neural differentiation in NSCs.

In addition, α-conotoxin AuIB, an inhibitor of $\alpha3\beta4$ nAChR, significantly decreased the expression of SOX2 and TuJ1 under OGD/R insult (Fig. S7). These findings might indicate that ACh activates the $\alpha3\beta4$ nAChR, which regulates the actions of the surrounding NSCs in the NSC niche.

4. Discussions

Our recent investigations revealed that DDAH1 might play protective roles in a variety of disorders, including cardiovascular diseases, hepatic dysfunction, airborne pollutants and Alzheimer's

Synapsin-1, Synaptophysin, PSD95 and GAP43 in the ipsilateral hippocampus 28 days after reperfusion injury. (K–N) Quantitative analysis of the expression of the presynaptic protein synapsin-1 (K), synaptophysin (L), the postsynaptic protein PSD95 (M) and the axon-guided protein GAP43 (N) in the ipsilateral hippocampus ($n = 3$ per group). The values are shown as the mean ± SEM. $^{\#}P < 0.05$, $^{\#\#}P < 0.01$ *versus* the WT group; one-way ANOVA with Dunnett's multiple comparisons test.

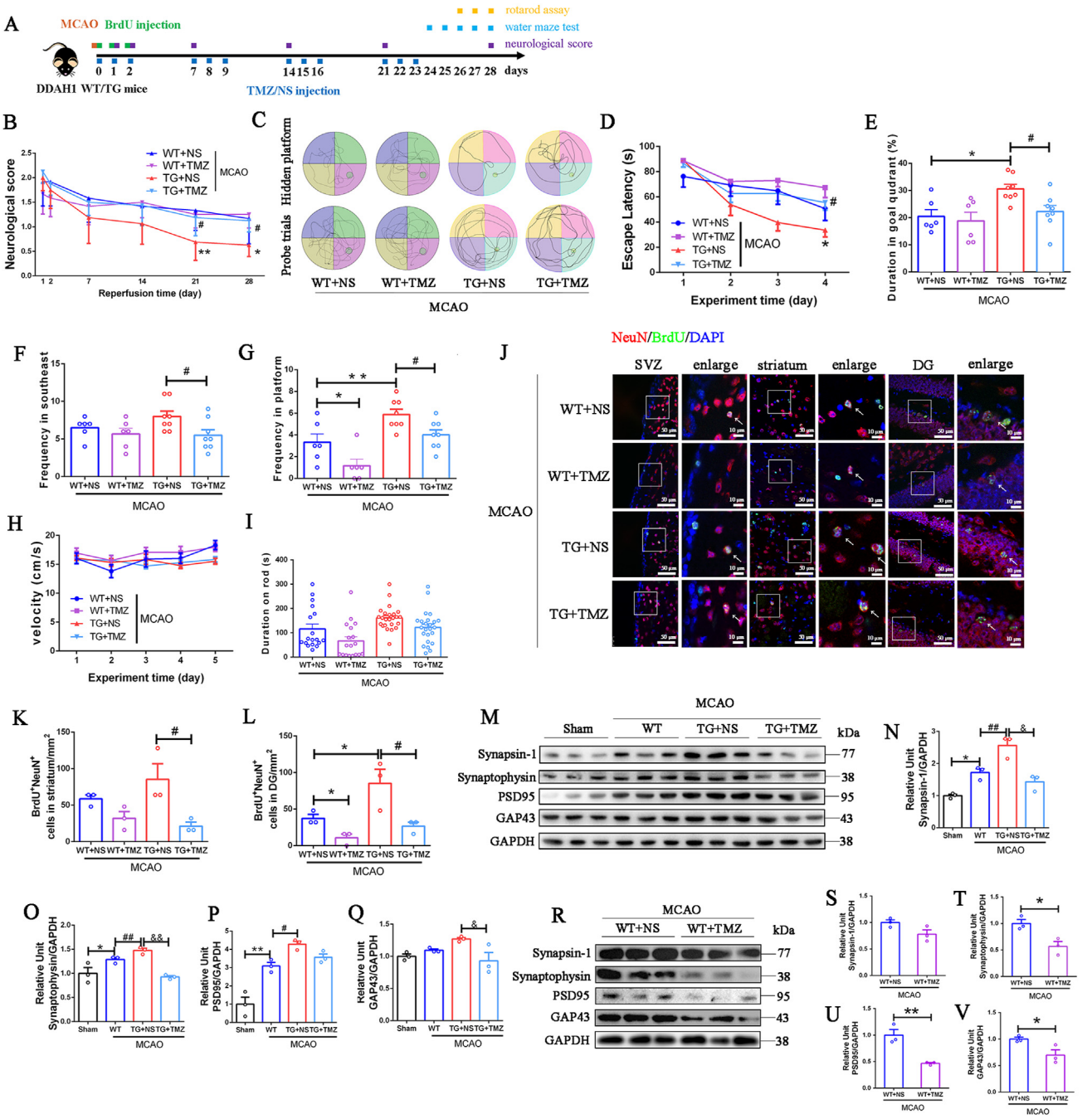

Figure 6 Poststroke neurogenesis enhanced by DDAH1 contributes to cognitive function recovery but not motor function recovery after I1h/R28d. (A) Experimental design for evaluating the influence of TMZ on cognitive functions and motor functions in *Ddah1* TG and WT mice after I1h/R28d insult. BrdU at a dosage of 50 mg/kg was administered twice a day for the first 2 days after ischemia. TMZ was injected during the first 3 days per week for 4 weeks at a dosage of 25 mg/kg during reperfusion. (B−H) Cognitive functions were evaluated by the Morris water maze test (n = 6, 6, 8, and 8 in WT+NS, WT+TMZ, TG+NS, and TG+TMZ groups, respectively). (B) Evaluation of neurological scores poststroke at the indicated times. The values are shown as the mean ± SEM. $^{*}P < 0.05$, $^{**}P < 0.01$ *versus* the WT+NS group; $^{\#}P < 0.05$ *versus* the TG+NS group. Two-way ANOVA with Dunnett's multiple comparisons test was used. (C) Representative swimming tracks to the hidden platform on Day 27 and the probe trial test on Day 28 poststroke. (D) Cognitive functions were assessed by the escape latency in the Morris water maze from Day 24 to Day 27 after ischemia. The values are shown as the mean ± SEM. $^{*}P < 0.05$ *versus* the WT+NS group; $^{\#}P < 0.05$ *versus* the TG+NS group; two-way ANOVA with Dunnett's multiple comparisons test. (E−G) Spatial bias (E), frequency in the southeastern quadrant (*i.e.*, platform-located quadrant) (F) and frequency on the platform (G) were detected in the probe trial survey on Day 28 after ischemia. (H) Swimming speed of mice within 5 days of the Morris water maze test. (I) Motor function was detected by the rotarod test. The latency to fall from the instrument was measured 3 times per mouse. (E−I) Values are shown as the mean ± SEM. $^{*}P < 0.05$, $^{**}P < 0.01$ *versus* the WT+NS group; $^{\#}P < 0.05$ *versus* the TG+NS group; one-way ANOVA with Dunnett's multiple comparisons test. (J) Representative images of double-label immunofluorescence staining for BrdU and NeuN in the ipsilateral SVZ, striatum and DG. (K, L) Statistical analysis of $BrdU^{+}NeuN^{+}$ cells in the ipsilateral striatum

disease[7,13,35,55,56]. Studies have shown that DDAH1 can attenuate blood−brain barrier leakage and improve cerebral ischemic tolerance in the early phase of cerebral ischemic stroke[14,16]. Thereafter, how DDAH1 varies in AIS patients and whether DDAH1 can induce a rehabilitative response to AIS insults need to be demonstrated. Our clinical study revealed that DDAH1 may be an endogenous protective factor against AIS since its increase is correlated with the severity of AIS impairment. DDAH1 might participate in cognitive and motor rehabilitation after experimental stroke impairment partially by activating endogenous hippocampal AN. After stroke insult, DDAH1 might activate multiple regeneration-guiding factors, including ChAT. ACh secreted from NSCs might promote the proliferation of adjacent NSCs through the $\alpha3\beta4$ nAChR receptor. In addition, DDAH1 might drive NSCs to differentiate into ChAT$^+$ neurons, which further activates the proliferation of surrounding NSCs. Enhanced neurogenic activity contributes to synapse formation and functional recovery against stroke impairment. In addition, the survival rates of the mice after 28 days of reperfusion were analyzed by χ^2 tests to determine whether DDAH1 could improve the survival rate after MCAO (Supporting Information Table S3). However, no significant difference was observed among the groups.

The microenvironments of the two discrete neurogenic niches, the SVZ and SGZ, play important roles in regulating the behavior of NSCs. Manipulating key factors from stem cell niches to stimulate endogenous NSCs to regenerate for poststroke brain repair is expected to be a potential neurogenic approach in stroke intervention[57,58]. Kozlova et al.[59] used specific markers of different types of cells to define the location of DDAH1 in the CNS. DDAH1 was found to be distributed in neurons, astrocytes and vascular endothelial cells in both mouse and human brains[60-62]. Does DDAH1 in endothelial cells or nerve cells play major roles in cell−cell communication and regulate neurogenic activity in the AN niche? To investigate this issue, we established a Nestin-Cre neural *Ddah1* cKO line and found that the neurogenic activity of *Ddah1* cKO mice was similar to that of DDAH general KO mice. Therefore, we propose that the major contributions of DDAH1 to the NSC niche are from nerve cells rather than from endothelial cells.

The neurotransmitter ACh can act as a niche-driven cue that controls neurogenesis in the SVZ and SGZ. ChAT$^+$ neurons in the SVZ niche can control the proliferation of NSCs[26], and ACh in the forebrain promotes the proliferation of NSCs in the SGZ[28]. How ACh and ChAT$^+$ neurons are derived should herein be demonstrated. In the present study, RNA sequencing analysis combined with real-time qPCR analysis and Western blot assay revealed that DDAH1 might regulate the key genes responsible for the synthesis of ACh (*Chat*, *Slc5a7*, *Slc18a3*) in the hippocampus after stroke onset. After ischemic insult, the expression of ChAT was significantly enhanced in the SGZ region (Figs. 8F, G and 9).

One limitation of our cKO model is that *Ddah1* is knocked out in embryonic NSCs. Considering that *Ddah1* might be knocked out in cells that might differentiate from NSCs (*e.g.*, neurons and astrocytes), isolated NSCs were applied to confirm the effects of DDAH1 on neurogenesis *in vitro*. *In vitro* assays revealed that DDAH1 controlled the expression of ChAT in NSCs and the further neurogenesis behavior of NSCs after OGD insult (Figs. S6 and S7). The concentration of ACh was significantly decreased in the *Ddah1* KO and cKO groups after stroke (Fig. 8K and R). Therefore, we propose that DDAH1 promotes the proliferation of NSCs by secreting ACh, which acts on adjacent NSCs. On the other hand, considering the results of the *in vitro* assay showing that DDAH1 could force NSCs to differentiate into ChAT$^+$ neurons, we speculated that ChAT$^+$ neurons differentiated by DDAH1 in turn induce the proliferation of surrounding NSCs.

The PC12 cell line is a simple and stable model for observing neural differentiation induced by NGF. Upon stimulation with NGF, PC12 cells start growing processes and differentiate into sympathetic-like neurons. NGF, which acts through the TrkA receptor, has been shown to regulate ACh production and storage by upregulating the expression of the ChAT and vesicular ACh transporter (VAChT) genes. These two genes are closely linked and share the regulatory sequences. Together, they form the so-called cholinergic locus[63]. In the present study, RNA-seq confirmed that DDAH1 regulated the genes *Chat* and *Slc18a3*. *Slc18a3* belongs to the VAChT family. Previous studies have shown that DDAH1 might regulate the expression of HIF-1α following ischemic insult[16]. Therefore, we predicted the potential effects of HIF-1α on *Chat* and *Slc18a3*. Bioinformatics analysis of the JASPAR database indicated that HIF-1α might act on the promoters of *Chat* and *Slc18a3*. The dual-luciferase reporter assay confirmed that DDAH1 enhanced the activity of ChAT, while this effect was abolished by treatment with KC7F2, an inhibitor of HIF-1α (Fig. S6). These results indicate that HIF-1α/*Chat* signaling might participate in DDAH1-promoted neurogenesis.

nAChRs are involved in various physiological and pathophysiological processes, including neuronal development. In our study, DDAH1 enhanced the expression of the $\alpha3$ and $\beta4$ subunits of nAChR receptors, which have been proven to play important roles in regeneration[32,63-70]. In the human hippocampus, subunits of $\alpha3$ and $\beta4$ are extensively expressed in pyramidal neurons, prealpha cells of the entorhinal cortex and dentate granule cells[64]. Gahring et al.[65] showed that the $\alpha3$ and $\beta4$ subunits were colo calized with glutamic acid decarboxylase (GAD)-positive interneurons in the mouse dorsal hippocampus. As reported, the $\alpha3\beta4$ subtype is the dominant functional nicotinic ACh receptor in neural progenitor cells in the rostral migratory stream (RMS). $\alpha3\beta4$ nAChR mediates calcium transients upon application of ACh in the RMS around the SVZ[32], while NGF increases the transcriptional activity of the $\beta4$ subunit[66]. The whole-cell ACh-

(K) and DG (L) ($n = 3$ per group). The values are shown as the mean ± SEM. $^*P < 0.05$ *versus* the WT+NS group; $^{\#}P < 0.05$ *versus* the TG+NS group; one-way ANOVA with Dunnett's multiple comparisons test. (M) Representative bands of Western blotting assays of the synapse-associated proteins synapsin-1, synaptophysin, PSD95 and GAP43 in the ipsilateral hippocampus of sham, TG+NS, and TG+TMZ groups after 28 days of reperfusion injury. (N−Q) Quantitative analysis of the expression of the presynaptic protein synapsin-1 (N), synaptophysin (O), PSD95 (P) and GAP43 (Q) in the ipsilateral hippocampus ($n = 3$ per group). The values are shown as the mean ± SEM. $^*P < 0.05$, $^{**}P < 0.01$ *versus* the sham group; $^{\#}P < 0.05$, $^{\#\#}P < 0.01$ *versus* the WT group; $^{\&}P < 0.05$, $^{\&\&}P < 0.01$ *versus* the TG+NS group; one-way ANOVA with Dunnett's multiple comparisons test. (R) Representative bands in Western blotting assays of synapsin-1, synaptophysin, PSD95 and GAP43 in the ipsilateral hippocampus of the WT+NS and WT+TMZ groups after 28 days of reperfusion injury. (S−V) Quantitative analysis of the expression of synapsin-1 (S), synaptophysin (T), PSD95 (U) and GAP43 (V) in the ipsilateral hippocampus ($n = 3$ per group). The values are shown as the mean ± SEM. $^*P < 0.05$ *versus* the WT+NS group; two-tailed Student's *t* test.

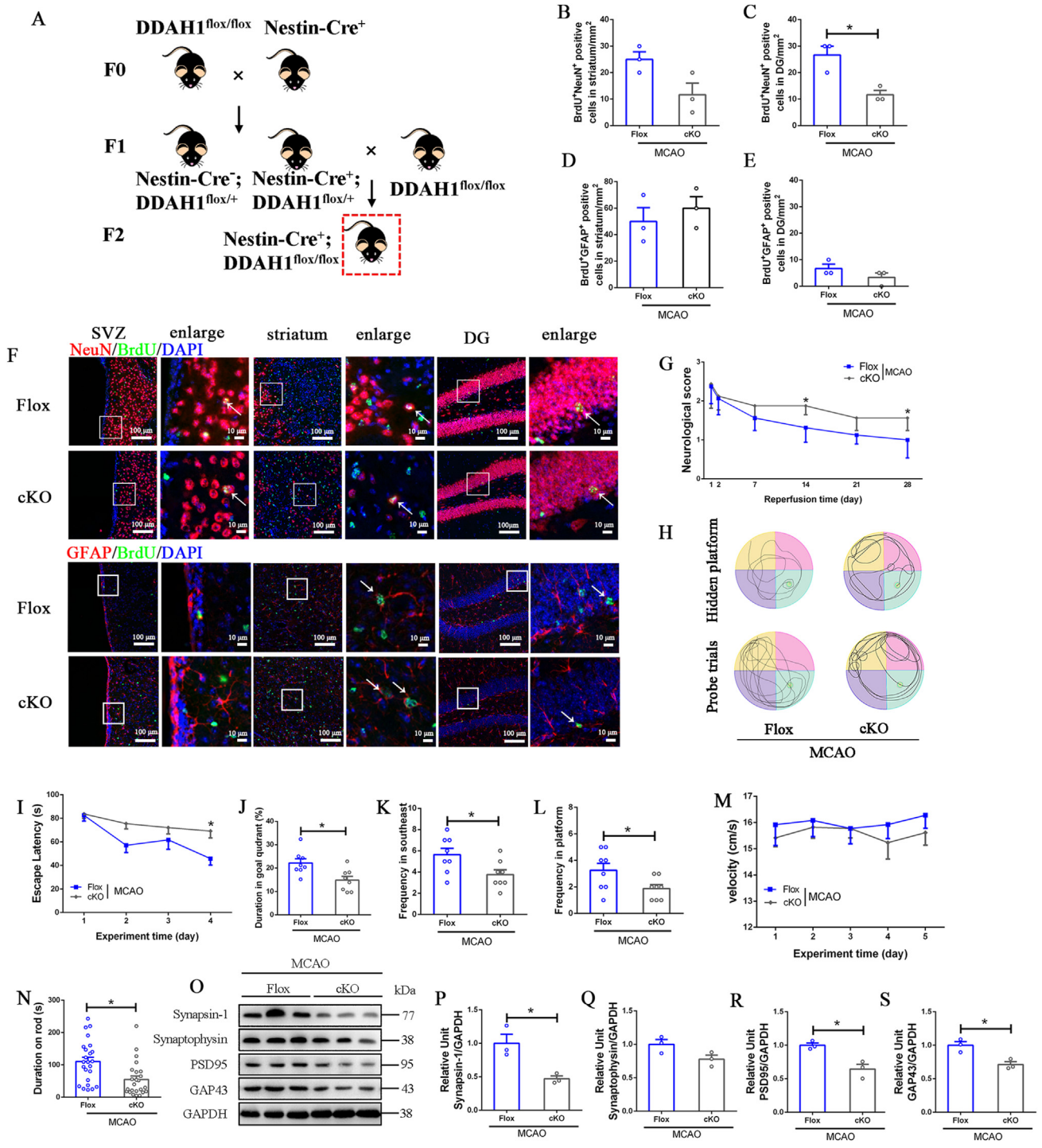

Figure 7 Conditional knockout of *Ddah1* in NSCs abolishes poststroke neurogenesis activities and exacerbates cognitive dysfunction. (A) Establishment of a Nestin-cre neural *Ddah1* conditional knockout (cKO; *Ddah1*$^{flox/flox}$; Nesin-Cre) mouse line. (B, C) Statistical analysis of immunofluorescence staining of BrdU^{+}NeuN^{+} cells in the ipsilateral striatum (B) and DG (C). (D, E) Statistical analysis of BrdU^{+}GFAP^{+} cells in the ipsilateral striatum (D) and DG (E). (B−E) Values are shown as the mean ± SEM. (n = 3 per group). *$P < 0.05$ *versus* the Flox group; two-tailed Student's t test. (F) Representative images of double-label immunofluorescence staining for BrdU and NeuN/GFAP in the ipsilateral SVZ, striatum and DG. (G) Evaluation of neurological deficits by the Longa scoring system poststroke at the indicated times (n = 8 per group). The values are shown as the mean ± SEM. *$P < 0.05$ *versus* the Flox group; two-way ANOVA with Dunnett's multiple comparisons test. (H) Representative swimming tracks to the hidden platform on Day 27 and the probe trial test on Day 28 poststroke. (I) Cognitive functions were assessed by the escape latency in the Morris water maze test from Day 24 to Day 27 after ischemia (n = 8 per group). The values are shown as the mean ± SEM. *$P < 0.05$ *versus* the Flox group; two-way ANOVA with Dunnett's multiple comparisons test. (J−L) Spatial bias (J), frequency in the southeastern quadrant (*i.e.*, platform-located quadrant) (K) and frequency on the platform (L) were detected on Day 28 in the probe trial survey after ischemia. (J−L) Values are shown as the mean ± SEM (n = 8 per group). *$P < 0.05$ *versus* the Flox group; two-tailed Student's t test. (M) Swimming speed of the mice within 5

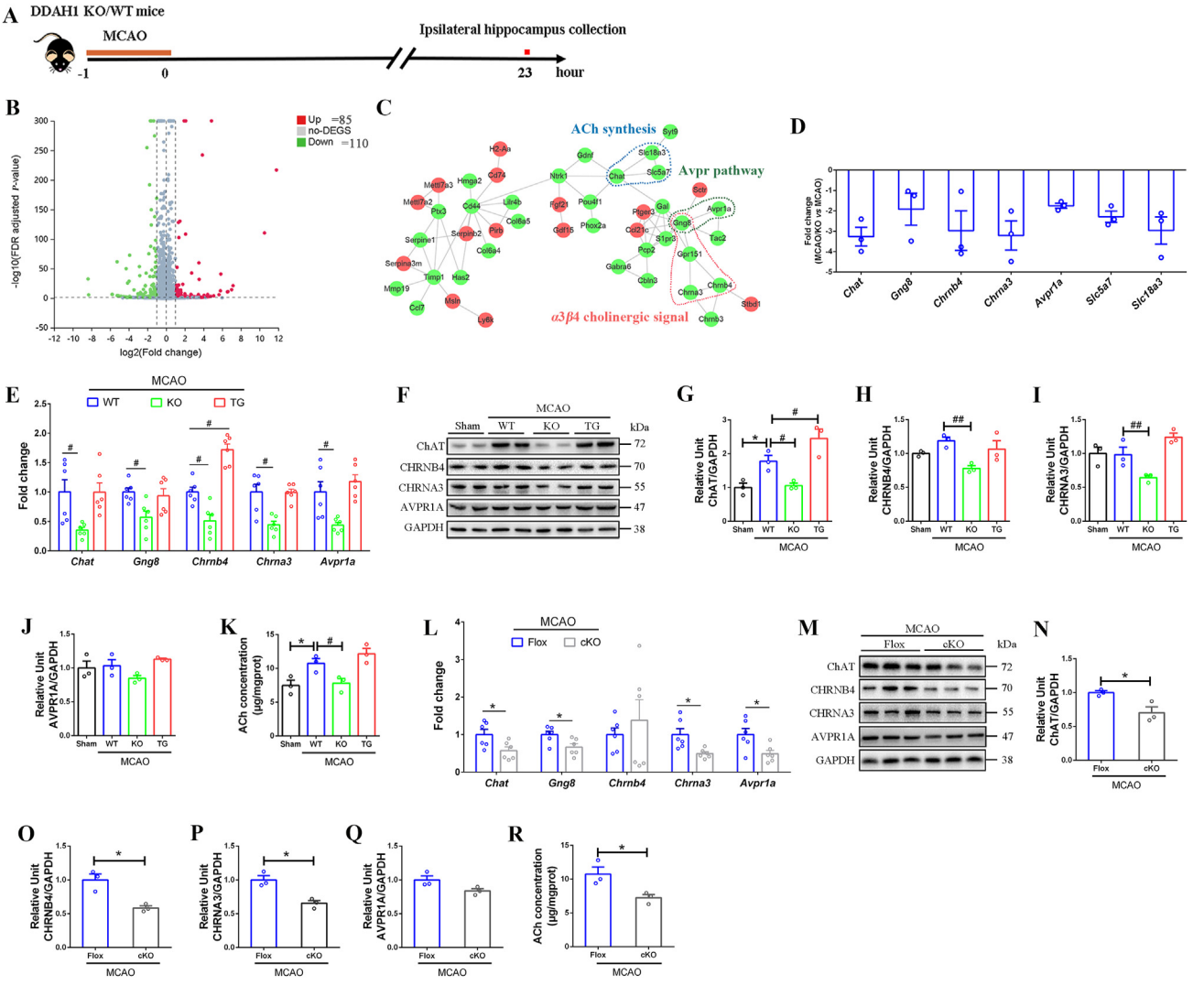

Figure 8 DEGs in the ipsilateral hippocampus were analyzed *via* RNA sequencing combined with bioinformatics and verified *via* real-time qPCR analysis and Western blot analysis. (A) Experimental illustration of the acute MCAO models for the detection of DEGs. Brain tissues from the ipsilateral hippocampus were collected for RNA sequencing analysis, real-time qPCR analysis and Western blot analysis after I1h/R23h. (B) Volcano map of DEGs from the ipsilateral hippocampus of Flox and *Ddah1* KO mice. Upregulated DEGs are labeled in red, and down-regulated DEGs are labeled in green. (C) PPI network of DEGs. The DEGs circled in blue were involved in ACh synthesis, those circled in red were involved in $\alpha3\beta4$ cholinergic signaling, and those circled in green were involved in the AVPR1A pathway. (D) RNA sequencing analysis of the key DEGs involved in cholinergic signaling and the AVPR1A pathway ($n = 3$ per group). (E) Identification of the expression of key DEGs in the cholinergic signaling pathway and AVPR1A pathway by real-time qPCR analysis in WT, KO and TG mice ($n = 6$ per group). The values are shown as the mean ± SEM. $^{\#}P < 0.05$ *versus* the WT group; one-way ANOVA with Dunnett's multiple comparisons test. (F) Representative dots of Western blot analysis showing cholinergic signals and the AVPR1A pathway in the ipsilateral hippocampus after I1h/R23h injury. (G−J) Quantitative analysis of the expression of representative proteins (*i.e.*, ChAT (G), CHRNB4 (H), CHRNA3 (I) and AVPR1A (J)) in the ipsilateral hippocampus. (K) ACh concentrations in the ipsilateral hippocampus were determined ($n = 3$ per group). The values are shown as the mean ± SEM. $^{*}P < 0.05$ *versus* the sham group; $^{\#}P < 0.05$, $^{\#\#}P < 0.01$ *versus* the WT group; one-way ANOVA with Dunnett's multiple comparisons test. (L) Identification of the expression of key DEGs by real-time qPCR analysis in Flox and cKO mice ($n = 6$ per group). (M−Q) Representative dots of Western blot analysis (M) and quantitative analysis of ChAT (N), CHRNB4 (O), CHRNA3 (P), and AVPR1A (Q) expression after I1h/R23h injury. (R) ACh concentrations in the ipsilateral hippocampus were determined ($n = 3$ per group). The values are shown as the mean ± SEM. $^{*}P < 0.05$ *versus* the Flox group; two-tailed Student's *t* test.

days of the Morris water maze test ($n = 8$ per group). The values are shown as the mean ± SEM. (N) Motor coordination was evaluated *via* the rotarod test. The latency to fall from the instrument was measured 3 times per mouse on Day 28 postischemia ($n = 8$ per group). The values are shown as the mean ± SEM. $^{*}P < 0.05$ *versus* the Flox group; two-tailed Student's *t* test. (O) Representative bands of Western blotting assays of the synapse-associated proteins Synapsin-1, Synaptophysin, PSD95 and GAP43 in the ipsilateral hippocampus 28 days after reperfusion injury. (P−S) Quanti tative analysis of the expression of synapsin-1 (P), synaptophysin (Q), PSD95 (R) and GAP43 (S) in the ipsilateral hippocampus ($n = 3$ per group). The values are shown as the mean ± SEM. $^{*}P < 0.05$ *versus* the Flox group; two-tailed Student's *t* test.

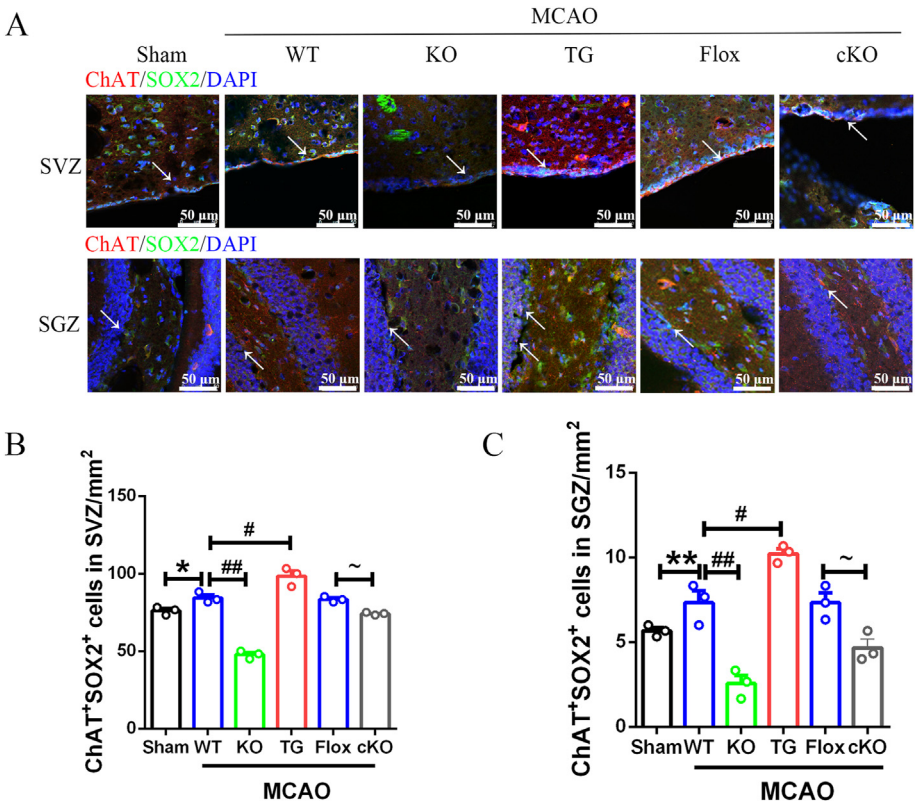

Figure 9 DDAH1 regulates the expression of ChAT localized in NSCs in the SVZ and SGZ 23 h after injury. (A) Representative images of double immunofluorescence staining for ChAT and SOX2 in the SVZ and SGZ. (B, C) Statistical analysis of $ChAT^+SOX2^+$ cells in the SVZ (B) and SGZ (C) ($n = 3$ per group). The values are shown as the mean ± SEM. $^*P < 0.05$, $^{**}P < 0.01$ *versus* the sham group; $^{\#}P < 0.05$, $^{\#\#}P < 0.01$ *versus* the WT group; $^{\sim}P < 0.05$ *versus* the Flox group; one-way ANOVA with Dunnett's multiple-comparison test.

evoked current of PC12 cells shows inward rectification[67,68]. Inward rectification is evoked by nicotinic receptors, including $\alpha3\beta4$[69]. P19 carcinoma embryonic cells act as another *in vitro* model of early neurogenesis. The presence of functional nAChRs, including $\alpha3$ and $\beta4$ subunits, in embryonic cells suggested that these receptors are involved in triggering Ca^{2+} waves during initial neuronal differentiation[70]. All these reports indicate that $\alpha3\beta4$ is a key factor in neurogenesis. Therefore, we deduced that DDAH1 might promote ACh-mediated neurogenesis through the $\alpha3\beta4$ nAChR. DDAH1 enhanced the synthesis of ACh in NSCs in the AN niche, as mediated by ACh. DDAH1 induced the proliferation of NSCs directly and indirectly by promoting the differentiation of NSCs into cholinergic neurons, which further stimulated the proliferation of the surrounding NSCs.

In our present study, we found that DDAH1 in NSCs regulated neurogenic behaviors after ischemic insult. The proliferation of NSCs in the SVZ and SGZ was promoted, but only the neuronal fate commitment of NSCs in the SGZ was determined (Figs. 3 and 4). Western blot analysis revealed that DDAH1 expression in the ipsilateral striatum increased but might reach a plateau when the duration of ischemia was extended. However, the expression of DDAH1 in the ipsilateral hippocampus was higher after 2 h of ischemia than after 1.5 h of ischemia (Fig. 2). Based on these observations, we speculated that DDAH1 might be controlled by negative feedback to prevent excess expression of DDAH1 in the ipsilateral striatum. This might lead the body to avoid overactivated neurogenesis and maintain NSC homeostasis in the SVZ. In addition, the role of DDAH1 in neurogenesis in normal mice was observed in our preliminary study. The results of $BrdU^+DCX^+$ and $BrdU^+NeuN^+$ colabeling indicated that knocking out DDAH1 tended to decrease neurogenic activity in the SGZ, while TG mice tended to increase neurogenic activity. However, no significant difference was observed among the groups. Based on these results, we speculated that DDAH1 might be involved in the regulation of NSC homeostasis *in vivo* so that its regulation of neurogenesis is confined to normal physical condition. The regulation of NSC homeostasis by DDAH1 after stroke insult will be explored in the future study.

BrdU incorporation is the classic assay for detecting neurogenesis, which is usually performed by labeling different biomarkers to identify cell types. GFAP is a biomarker that can be used to identify astrocytes. However, it can also be expressed in the early phase of NSCs[71]. To further confirm that $BrdU^+GFAP^+$ cells are newborn astrocytes that differentiate from NSCs, we performed BrdU/S100β/GFAP costaining of brain sections subjected to 28 days of ischemia. As reported, S100β is a 'mature' astrocyte biomarker that eliminates the potential for NSCs[72,73]. In our present study, S100β could stain almost all of the $BrdU^+GFAP^+$ cells, indicating that the $BrdU^+GFAP^+$ cells after 28 days of ischemic insult represented astrocytes differentiated from NSCs (Fig. S8).

In addition to its ability to activate cholinergic signals, we explored the regulation of DDAH1 on the canonical DDAH1/ADMA/NOS pathway after stroke insult. NO originating from endothelial NOS (eNOS) improves rCBF in the penumbra of the ischemic brain[74]. In the present study, the rCBFs of the ischemic

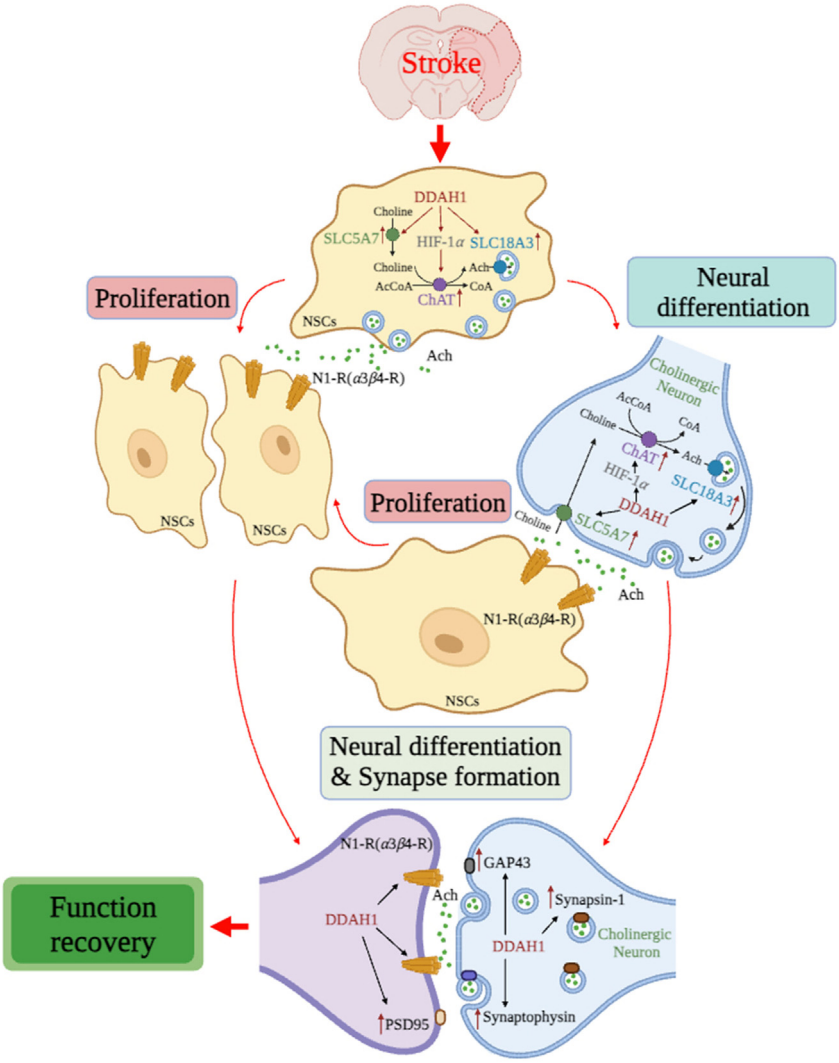

Figure 10 Illustration summarizing the effects of DDAH1 on neurogenesis and rehabilitation functions after ischemic stroke and the underlying mechanism involved. After stroke insult, elevated DDAH1 regulates the genes responsible for the synthesis of ACh (*Chat*, *Slc5a7* and *Slc18a3*) and the concentration of ACh in the hippocampus. The synthesis of ACh might be controlled by the transcription factor HIF-1α. Mediated by ACh, DDAH1 plays an important role in the AN niche, which might directly induce the proliferation of NSCs and indirectly promote the differentiation of NSCs into cholinergic neurons. These cascades might further stimulate the proliferation of surrounding NSCs. Enhanced neurogenic activity contributes to synapse formation and cognitive and motor functional recovery against stroke impairment.

region were detected during and after ischemia (Fig. S9). The results show that the rCBF decreased to approximately 20% of the baseline before MCAO, indicating that the middle cerebral artery (MCA) was successfully occluded. The rCBFs of *Ddah1* TG mice were slightly improved at 60 min after ischemia, while there were no significant differences among the WT, KO and TG mice after 20 min of reperfusion, indicating that the regulation of rCBFs by DDAH1 was slight and moderate (Fig. S9B and S9C).

In the present study, the NO concentration was investigated by immunostaining for 3-NT, the peroxynitrite metabolite of NO[75]. The concurrent consequence was that DDAH1 elevated the NO level in both the SVZ and the SGZ at the early reperfusion stage (Fig. S9D–S9F). It was proposed that the enhancement of rCBF regulated by DDAH1 might produce protective effects against acute ischemic insults. The results indicate that DDAH1 regulated neurological disorders and the infarction volume after ischemic insult (Fig. S9G–S9I). Compared with WT mice, *Ddah1* KO mice exhibited more severe neurological deficits and larger infarction, while TG mice exhibited the opposite trends.

In addition to providing acute neuroprotection against ischemic insults, NO can induce NSCs to proliferate and differentiate into neural cells by regulating the expression of VEGF[76]. Therefore, DDAH1 might also promote regenerative actions by regulating the synthesis of NO. In addition to regulating cholinergic signals and the NOS/NO pathway, DDAH1 might promote regenerative actions through other signals. As described, DDAH1 may have a mild regulatory effect on AVPR1A receptor expression, which also results in neuroprotection against degenerative insults[77]. However, further research should be performed to address these questions.

5. Conclusions

In summary, DDAH1 regulates the genes responsible for the synthesis of ACh (*Chat*, *Slc5a7*, *Slc18a3*) and the concentration of ACh in the hippocampus after stroke insult as illustrated in Fig. 10. Mediated by ACh, DDAH1 plays an important role in the AN niche, which might directly induce the proliferation of NSCs and indirectly promote the differentiation of NSCs into cholinergic neurons that further stimulate the proliferation of the sur rounding NSCs. Enhanced neurogenic activity contributes to synapse formation and functional recovery against stroke impairment. Therefore, DDAH1 may be a promising drug target for stroke intervention.

Acknowledgments

This work was supported by the National Natural Science Foundation of China (32171237, 82070250, 82171301, 82370275, 32071126), Beijing Natural Science Foundation (7222010) and the Fundamental Research Funds for the Central Universities. Thanks for the support of the undergraduate research training programs of Capital Medical University (XSKY2023, XSKY2022, XSKY2021), China. We sincerely acknowledged that Professor Jianwei Jiao from the Institute of Zoology, Chinese Academy of Sciences, kindly provided the Nestin-Cre (C57BL/6. Cg-Tg (Nes-Cre)1Kln/J) mice. We sincerely appreciate for the technical service and support from Tissue Gnostics Asia Pacific Limited in the image caption and data analysis of immunohistochemical staining analysis.

Author contributions

Yuming Zhao was the principal architect of the project, devising the experiments and revising the manuscript. Zhongbing Lu was pivotal in design and analysis of DDAH1 organism and the RNA-seq assay. Yumin Luo was pivotal in design and data analysis of clinical study. Ming Xue, Yang Liu, Xiaoyan Feng and Teng Zhang guided the experiments. Qiming Gao, Pinfei Ni and Yilin Wang were pivotal researchers who performed the *in vivo* study, *in vitro* study and the clinical study, respectively. Peiyun Huo, Xiaojie Zhang, Sihan Wang, Fuyao Xiao, Yixuan Li, Boyu Fan, Yuhao Kan, Yimiao Qi, Junfei Xing, Haixiao Cheng, Xinran Gao, Zhirui Li, Zhenhong Yang, Wei Feng, Juntao Yuan, Qiang Li performed experiments. Qiming Gao, Pinfei Ni and Yilin Wang wrote the manuscript. All the authors read and approved the final manuscript.

Conflicts of interest

The authors declare that there is no conflict of interest.

Appendix A. Supporting information

Supporting data to this article can be found online at https://doi.org/10.1016/j.apsb.2024.02.001.

References

1. Roth GA, Mensah GA, Johnson CO, Addolorato G, Ammirati E, Baddour LM, et al. Global burden of cardiovascular diseases and risk factors, 1990–2019: update from the GBD 2019 study. *J Am Coll Cardiol* 2020;**76**:2982–3021.
2. Zhang Y, Zhang H, Zhao F, Jiang Z, Cui Y, Ou M, et al. Mitochondrial-targeted and ROS-responsive nanocarrier *via* nose-to-brain pathway for ischemic stroke treatment. *Acta Pharm Sin B* 2023;**13**:5107–20.
3. Feigin VL, Norrving B, Mensah GA. Global burden of stroke. *Circ Res* 2017;**120**:439–48.
4. Katan M, Luft A. Global burden of stroke. *Semin Neurol* 2018;**38**:208–11.
5. Donkor ES. Stroke in the 21st century: a snapshot of the burden, epidemiology, and quality of life. *Stroke Res Treat* 2018;**2018**:3238165.
6. Wang S, Wang R, Meng N, Lu L, Wang J, Zhou J, et al. Engineered platelets-based drug delivery platform for targeted thrombolysis. *Acta Pharm Sin B* 2022;**12**:2000–13.
7. Hu X, Atzler D, Xu X, Zhang P, Guo H, Lu Z, et al. Dimethylarginine dimethylaminohydrolase-1 is the critical enzyme for degrading the cardiovascular risk factor asymmetrical dimethylarginine. *Arterioscler Thromb Vasc Biol* 2011;**31**:1540–6.
8. Ito A, Tsao PS, Adimoolam S, Kimoto M, Ogawa T, Cooke JP. Novel mechanism for endothelial dysfunction: dysregulation of dimethylarginine dimethylaminohydrolase. *Circulation* 1999;**99**:3092–5.
9. Lu TM, Lin SJ, Lin MW, Hsu CP, Chung MY. The association of dimethylarginine dimethylaminohydrolase 1 gene polymorphism with type 2 diabetes: a cohort study. *Cardiovasc Diabetol* 2011;**10**:16.
10. Stuhlinger MC, Tsao PS, Her JH, Kimoto M, Balint RF, Cooke JP. Homocysteine impairs the nitric oxide synthase pathway: role of asymmetric dimethylarginine. *Circulation* 2001;**104**:2569–75.
11. Shen X, Luo K, Yuan J, Gao J, Cui B, Yu Z, et al. Hepatic DDAH1 mitigates hepatic steatosis and insulin resistance in obese mice: involvement of reduced S100A11 expression. *Acta Pharm Sin B* 2023;**13**:3352–64.
12. MacAllister RJ, Parry H, Kimoto M, Ogawa T, Russell RJ, Hodson H, et al. Regulation of nitric oxide synthesis by dimethylarginine dimethylaminohydrolase. *Br J Pharmacol* 1996;**119**:1533–40.
13. Xu X, Zhang P, Kwak D, Fassett J, Yue W, Atzler D, et al. Cardiomyocyte dimethylarginine dimethylaminohydrolase-1 (DDAH1) plays an important role in attenuating ventricular hypertrophy and dysfunction. *Basic Res Cardiol* 2017;**112**:55.
14. Zhao Y, Ma X, Zhou Y, Xie J, Liu X, Zhao Y. DDAH-1, *via* regulation of ADMA levels, protects against ischemia-induced blood–brain barrier leakage. *Lab Invest* 2021;**101**:808–23.
15. Ding H, Wu B, Wang H, Lu Z, Yan J, Wang X, et al. A novel loss-of-function DDAH1 promoter polymorphism is associated with increased susceptibility to thrombosis stroke and coronary heart disease. *Circ Res* 2010;**106**:1145–52.
16. Zhao Y, Zhou Y, Ma X, Liu X, Zhao Y, Liu X. DDAH-1 *via* HIF-1 target genes improves cerebral ischemic tolerance after hypoxic preconditioning and middle cerebral artery occlusion–reperfusion. *Nitric Oxide* 2020;**95**:17–28.
17. Zhao Y, Zhang M, Dou Y, Du K, Liu X, Zhao Y. DDAH1/ADMA regulates adiponectin resistance in cerebral ischemia *via* the ROS/FOXO1/APR1 pathway. *Oxid Med Cell Longev* 2022;**2022**:2350857.
18. Wang S, Hu CP, Yuan Q, Zhang WF, Zhou Z, Nie SD, et al. Dimethylarginine dimethylaminohydrolase 1 regulates nerve growth factorpromoted differentiation of PC12 cells in a nitric oxide-dependent but asymmetric dimethylargenine-independent manner. *J Neurosci Res* **90**:1209–17.
19. Choi SH, Bylykbashi E, Chatila ZK, Lee SW, Pulli B, Clemenson GD, et al. Combined adult neurogenesis and BDNF mimic exercise effects on cognition in an Alzheimer's mouse model. *Science* 2018;**361**:eaan8821.
20. Yousef H, Czupalla CJ, Lee D, Chen MB, Burke AN, Zera KA, et al. Aged blood impairs hippocampal neural precursor activity and activates microglia *via* brain endothelial cell VCAM1. *Nat Med* 2019;**25**:988–1000.
21. Ayoub R, Ruddy RM, Cox E, Oyefiade A, Derkach D, Laughlin S, et al. Assessment of cognitive and neural recovery in survivors of

pediatric brain tumors in a pilot clinical trial using metformin. *Nat Med* 2020;**26**:1285−94.
22. Imayoshi I, Sakamoto M, Ohtsuka T, Takao K, Miyakawa T, Yamaguchi M, et al. Roles of continuous neurogenesis in the structural and functional integrity of the adult forebrain. *Nat Neurosci* 2008;**11**:1153−61.
23. Sahay A, Scobie KN, Hill AS, O'Carroll CM, Kheirbek MA, Burghardt NS, et al. Increasing adult hippocampal neurogenesis is sufficient to improve pattern separation. *Nature* 2011;**472**:466−70.
24. Shors TJ, Miesegaes G, Beylin A, Zhao M, Rydel T, Gould E. Neurogenesis in the adult is involved in the formation of trace memories. *Nature* 2001;**410**:372−6.
25. Sharma P, Mesci P, Carromeu C, McClatchy DR, Schiapparelli L, Yates JR 3rd, et al. Exosomes regulate neurogenesis and circuit assembly. *Proc Natl Acad Sci U S A* 2019;**116**:16086−94.
26. Paez-Gonzalez P, Asrican B, Rodriguez E, Kuo CT. Identification of distinct ChAT^{+} neurons and activity-dependent control of postnatal SVZ neurogenesis. *Nat Neurosci* 2014;**17**:934−42.
27. Pilz GA, Jessberger S. ChAT me up: how neurons control stem cells. *Nat Neurosci* 2014;**17**:897−8.
28. Mohapel P, Leanza G, Kokaia M, Lindvall O. Forebrain acetylcholine regulates adult hippocampal neurogenesis and learning. *Neurobiol Aging* 2005;**26**:939−46.
29. Veena J, Srikumar BN, Mahati K, Raju TR, Shankaranarayana Rao BS. Oxotremorine treatment restores hippocampal neurogenesis and ameliorates depression-like behaviour in chronically stressed rats. *Psychopharmacology (Berl)* 2011;**217**:239−53.
30. Wang J, Lu Z, Fu X, Zhang D, Yu L, Li N, et al. Alpha-7 nicotinic receptor signaling pathway participates in the neurogenesis induced by ChAT-positive neurons in the subventricular zone. *Transl Stroke Res* 2017;**8**:484−93.
31. Theisen U, Hennig C, Ring T, Schnabel R, Koster RW. Neurotransmitter-mediated activity spatially controls neuronal migration in the zebrafish cerebellum. *PLoS Biol* 2018;**16**:e2002226.
32. Sharma G. The dominant functional nicotinic receptor in progenitor cells in the rostral migratory stream is the $\alpha 3\beta 4$ subtype. *J Neurophysiol* 2013;**109**:867−72.
33. Zhao H, Li F, Huang Y, Zhang S, Li L, Yang Z, et al. Prognostic significance of plasma IL-2 and sIL-2Rα in patients with first-ever ischaemic stroke. *J Neuroinflammation* 2020;**17**:237.
34. Zheng Y, Huang Y, Li L, Wang P, Wang R, Tao Z, et al. sLOX-1: a molecule for evaluating the prognosis of recurrent ischemic stroke. *Neural Plast* 2021;**2021**:6718184.
35. Li T, Feng R, Zhao C, Wang Y, Wang J, Liu S, et al. Dimethylarginine dimethylaminohydrolase 1 protects against high-fat diet-induced hepatic steatosis and insulin resistance in mice. *Antioxid Redox Signal* 2017;**26**:598−609.
36. Ji F, Wang W, Feng C, Gao F, Jiao J. Brain-specific Wt1 deletion leads to depressive-like behaviors in mice *via* the recruitment of Tet2 to modulate Epo expression. *Mol Psychiatry* 2021;**26**:4221−33.
37. Cheng Y, Wang ZM, Tan W, Wang X, Li Y, Bai B, et al. Partial loss of psychiatric risk gene *Mir137* in mice causes repetitive behavior and impairs sociability and learning *via* increased *Pde10a*. *Nat Neurosci* 2018;**21**:1689−703.
38. Longa EZ, Weinstein PR, Carlson S, Cummins R. Reversible middle cerebral artery occlusion without craniectomy in rats. *Stroke* 1989;**20**:84−91.
39. Cai Q, Xu G, Liu J, Wang L, Deng G, Liu J, et al. A modification of intraluminal middle cerebral artery occlusion/reperfusion model for ischemic stroke with laser Doppler flowmetry guidance in mice. *Neuropsychiatr Dis Treat* 2016;**12**:2851−8.
40. Zhao Y, Li W, Chow PCY, Lau DTK, Lee NTK, Pang Y, et al. Bis(7)-tacrine, a promising anti-Alzheimer's dimer, affords dose- and time-dependent neuroprotection against transient focal cerebral ischemia. *Neurosci Lett* 2008;**439**:160−4.
41. Luo Y, Huang C, Zhao Y, Zhang L, Li M, Li Y, et al. Dynamic detection of specific membrane capacitance and cytoplasmic resistance of neutrophils after ischemic stroke. *Aging Dis* 2023;**14**:1035−7.
42. Wang R, Zhang S, Yang Z, Zheng Y, Yan F, Tao Z, et al. Mutant erythropoietin enhances white matter repair *via* the JAK2/STAT3 and C/EBPβ pathway in middle-aged mice following cerebral ischemia and reperfusion. *Exp Neurol* 2021;**337**:113553.
43. Wang S, Lv W, Zhang H, Liu Y, Li L, Jefferson JR, et al. Aging exacerbates impairments of cerebral blood flow autoregulation and cognition in diabetic rats. *Geroscience* 2020;**42**:1387−410.
44. Wojtowicz JM, Kee N. BrdU assay for neurogenesis in rodents. *Nat Protoc* 2006;**1**:1399−405.
45. Xiao F, Zhang X, Ni P, Yu H, Gao Q, Li M, et al. Voltage-dependent potassium channel Kv4.2 alleviates the ischemic stroke impairments through activating neurogenesis. *Neurochem Int* 2021;**150**:105155.
46. Chen J, Li Y, Yu TS, McKay RM, Burns DK, Kernie SG, et al. A restricted cell population propagates glioblastoma growth after chemotherapy. *Nature* 2012;**488**:522−6.
47. Song W, Bai L, Yang Y, Wang Y, Xu P, Zhao Y, et al. Long-circulation and brain targeted isoliquiritigenin micelle nanoparticles: formation, characterization, tissue distribution, pharmacokinetics and effects for ischemic stroke. *Int J Nanomedicine* 2022;**17**:3655−70.
48. Zhao Y, Xu P, Hu S, Du L, Xu Z, Zhang H, et al. Tanshinone II A, a multiple target neuroprotectant, promotes caveolae-dependent neuronal differentiation. *Eur J Pharmacol* 2015;**765**:437−46.
49. Wu Y, Hu Y, Wang B, Li S, Ma C, Liu X, et al. Dopamine uses the DRD5−ARRB2−PP2A signaling axis to block the TRAF6-mediated NF-κB pathway and suppress systemic inflammation. *Mol Cell* 2020;**78**:42−56.
50. Zhou Y, Zhou B, Pache L, Chang M, Khodabakhshi AH, Tanaseichuk O, et al. Metascape provides a biologist-oriented resource for the analysis of systems-level datasets. *Nat Commun* 2019;**10**:1523.
51. Domi E, Caputi FF, Romualdi P, Domi A, Scuppa G, Candeletti S, et al. Activation of PPARγ attenuates the expression of physical and affective nicotine withdrawal symptoms through mechanisms involving amygdala and hippocampus neurotransmission. *J Neurosci* 2019;**39**:9864−75.
52. Zhao Y, Liu D, Li J, Zhang X, Wang X. L-NBP, A multiple growth factor activator, attenuates ischemic neuronal impairments possibly through promoting neuritogenesis. *Neurochem Int* 2019;**124**:94−105.
53. Santamaria J, Khalfallah O, Sauty C, Brunet I, Sibieude M, Mallet J, et al. Silencing of choline acetyltransferase expression by lentivirus-mediated RNA interference in cultured cells and in the adult rodent brain. *J Neurosci Res* 2009;**87**:532−44.
54. Xu X, Fan S, Zhou J, Zhang Y, Che Y, Cai H, et al. The mutated tegument protein UL7 attenuates the virulence of herpes simplex virus 1 by reducing the modulation of α-4 gene transcription. *Virol J* 2016;**13**:152.
55. Luo Y, Yue W, Quan X, Wang Y, Zhao B, Lu Z. Asymmetric dimethylarginine exacerbates Aβ-induced toxicity and oxidative stress in human cell and *Caenorhabditis elegans* models of Alzheimer disease. *Free Radic Biol Med* 2015;**79**:117−26.
56. Wang H, Guo Y, Liu L, Guan L, Wang T, Zhang L, et al. DDAH1 plays dual roles in PM2.5 induced cell death in A549 cells. *Biochim Biophys Acta* 2016;**1860**:2793−801.
57. Goncalves JT, Schafer ST, Gage FH. Adult neurogenesis in the hippocampus: from stem cells to behavior. *Cell* 2016;**167**:897−914.
58. Wu KJ, Yu S, Lee JY, Hoffer B, Wang Y. Improving neurorepair in stroke brain through endogenous neurogenesis-enhancing drugs. *Cell Transplant* 2017;**26**:1596−600.
59. Kozlova AA, Ragavan VN, Jarzebska N, Lukianova IV, Bikmurzina AE, Rubets E, et al. Divergent dimethylarginine dimethylaminohydrolase isoenzyme expression in the central nervous system. *Cell Mol Neurobiol* 2022;**42**:2273−88.
60. Wang Y, Wang E, Zhang Y, Madamsetty VS, Ji B, Radisky DC, et al. Neuropilin-1 maintains dimethylarginine dimethylaminohydrolase 1 expression in endothelial cells, and contributes to protection from angiotensin II-induced hypertension. *FASEB J* 2019;**33**:494−500.
61. Pullamsetti S, Kiss L, Ghofrani HA, Voswinckel R, Haredza P, Klepetko W, et al. Increased levels and reduced catabolism of asymmetric and symmetric dimethylarginines in pulmonary hypertension. *FASEB J* 2005;**19**:1175−7.

62. Jacobi J, Sydow K, von Degenfeld G, Zhang Y, Dayoub H, Wang B, et al. Overexpression of dimethylarginine dimethylaminohydrolase reduces tissue asymmetric dimethylarginine levels and enhances angiogenesis. *Circulation* 2005;**111**:1431−8.
63. Eiden LE. The cholinergic gene locus. *J Neurochem* 1998;**70**:2227−40.
64. Graham AJ, Ray MA, Perry EK, Jaros E, Perry RH, Volsen SG, et al. Differential nicotinic acetylcholine receptor subunit expression in the human hippocampus. *J Chem Neuroanat* 2003;**25**:97−113.
65. Gahring LC, Persiyanov K, Dunn D, Weiss R, Meyer EL, Rogers SW. Mouse strain-specific nicotinic acetylcholine receptor expression by inhibitory interneurons and astrocytes in the dorsal hippocampus. *J Comp Neurol* 2004;**468**:334−46.
66. Hu M, Whiting Theobald NL, Gardner PD. Nerve growth factor increases the transcriptional activity of the rat neuronal nicotinic acetylcholine receptor β 4 subunit promoter in transfected PC12 cells. *J Neurochem* 1994;**62**:392−5.
67. Ifune CK, Steinbach JH. Inward rectification of acetylcholine-elicited currents in rat phaeochromocytoma cells. *J Physiol* 1992;**457**:143−65.
68. Sands SB, Barish ME. Neuronal nicotinic acetylcholine receptor currents in phaeochromocytoma (PC12) cells: dual mechanisms of rectification. *J Physiol* 1992;**447**:467−87.
69. Haghighi AP, Cooper E. A molecular link between inward rectification and calcium permeability of neuronal nicotinic acetylcholine $\alpha 3\beta 4$ and $\alpha 4\beta 2$ receptors. *J Neurosci* 2000;**20**:529−41.
70. Resende RR, Gomes KN, Adhikari A, Britto LR, Ulrich H. Mechanism of acetylcholine-induced calcium signaling during neuronal differentiation of P19 embryonal carcinoma cells *in vitro*. *Cell Calcium* 2008;**43**:107−21.
71. Ming G, Song H. Adult neurogenesis in the mammalian central nervous system. *Annu Rev Neurosci* 2005;**28**:223−50.
72. Nygren J, Wieloch T, Pesic J, Brundin P, Deierborg T. Enriched environment attenuates cell genesis in subventricular zone after focal ischemia in mice and decreases migration of newborn cells to the striatum. *Stroke* 2006;**37**:2824−9.
73. Raponi E, Agenes F, Delphin C, Assard N, Baudier J, Legraverend C, et al. S100B expression defines a state in which GFAP-expressing cells lose their neural stem cell potential and acquire a more mature developmental stage. *Glia* 2007;**55**:165−77.
74. Morikawa E, Moskowitz MA, Huang Z, Yoshida T, Irikura K, Dalkara T. L-Arginine infusion promotes nitric oxide-dependent vasodilation, increases regional cerebral blood flow, and reduces infarction volume in the rat. *Stroke* 1994;**25**:429−35.
75. Zhao Y, Huang Y, Fang Y, Zhao H, Shi W, Li J, et al. Chrysophanol attenuates nitrosative/oxidative stress injury in a mouse model of focal cerebral ischemia/reperfusion. *J Pharmacol Sci* 2018;**138**:16−22.
76. Fabel K, Fabel K, Tam B, Kaufer D, Baiker A, Simmons N, et al. VEGF is necessary for exercise-induced adult hippocampal neurogenesis. *Eur J Neurosci* 2003;**18**:2803−12.
77. Lei S, Hu B, Rezagholizadeh N. Activation of V1a vasopressin receptors excite subicular pyramidal neurons by activating TRPV1 and depressing GIRK channels. *Neuropharmacology* 2021;**190**:108565.